University of Reading

Structural, functional and mechanistic insights uncover the fundamental role of orphan connexin-62 in platelets

Article

Accepted Version

Sahli, K. A., Flora, G. D., Sasikumar, P., Maghrabi, A. H., Holbrook, L., AlOuda, S. K., Elgheznawy, A., Sage, T., Stainer, A. R., Adiyaman, R., AboHassan, M., Crescente, M., Kriek, N., Vaiyapuri, S. ORCID: https://orcid.org/0000-0002-6006-6517, Bye, A. P. ORCID: https://orcid.org/0000-0002-2061-2253, Unsworth, A. J., Jones, C. I. ORCID: https://orcid.org/0000-0001-7537-1509, McGuffin, L. J. ORCID: https://orcid.org/0000-0003-4501-4767 and Gibbins, J. M. ORCID: https://orcid.org/0000-0002-0372-5352 (2021) Structural, functional and mechanistic insights uncover the fundamental role of orphan connexin-62 in platelets. Blood, 137 (6). pp. 830-843. ISSN 0006-4971 doi: 10.1182/blood.2019004575 Available at https://centaur.reading.ac.uk/92331/

It is advisable to refer to the publisher's version if you intend to cite from the work. See Guidance on citing.

To link to this article DOI: http://dx.doi.org/10.1182/blood.2019004575

Publisher: American Society of Hematology

University of Reading

All outputs in CentAUR are protected by Intellectual Property Rights law, including copyright law. Copyright and IPR is retained by the creators or other copyright holders. Terms and conditions for use of this material are defined in the End User Agreement.

www.reading.ac.uk/centaur

CentAUR

Central Archive at the University of Reading

Reading's research outputs online

Regular Article

Structural, Functional and Mechanistic Insights Uncover the Fundamental Role of Orphan Connexin62 in Platelets

Authors:

Khaled A. Sahli,[1,2 *] Gagan D. Flora,[1,3 *] Parvathy Sasikumar,[1,4] Ali H. Maghrabi,[1] Lisa-Marie Holbrook,[1,5], Sarah K. AlOuda,[1] Amro Elgheznawy[1], Tanya Sage,[1] Alexander R. Stainer,[1] Recep Adiyaman,[1] Mohammad AboHassan,[1] Marilena Crescente,[1,6] Neline Kriek[1], Sakthivel Vaiyapuri[1,7], Alexander P. Bye,[1] Amanda J. Unsworth[1,8], Christopher I. Jones[1], Liam J. McGuffin,[1] Jonathan M. Gibbins[1]

[1]Institute for Cardiovascular and Metabolic Research, School of Biological Sciences, University of Reading, UK
[2]General Directorate of Medical Services, Ministry of Interior, Riyadh, KSA
[3]Department of Internal Medicine, University of Iowa, Iowa City, IA, USA
[4]Centre for Haematology, Imperial College London, Hammersmith Hospital Campus, UK†
[5]School of Cardiovascular Medicine and Sciences, King's College London, London, UK
[6]Centre for Immunobiology, Blizard Institute, Barts and The London School of Medicine and Dentistry, Queen Mary University of London, UK
[7]School of Pharmacy, University of Reading, UK
[8]Department of Life Sciences, School of Science and Engineering, Manchester Metropolitan University, Manchester, UK

Correspondence: j.m.gibbins@reading.ac.uk

[*]KAS and GDF contributed equally to this study and are joint first authors

Short title: Role of Orphan Connexin62 in Platelets

Word count: 4735

Abstract word count: 183

Key Points

- Cx62 is present in platelets and its inhibitor (^{62}Gap27) attenuates hemichannel and gap junction-mediated intercellular communication
- ^{62}Gap27 inhibited platelet function, thrombosis and haemostasis via upregulation of inhibitory PKA signalling in platelets.

Abstract

Connexins (Cxs) oligomerise to form hexameric hemichannels in the plasma membrane that can further dock together on adjacent cells to form gap junctions and facilitate intercellular-trafficking of molecules. In this study, we report the expression and function of an 'orphan' connexin, Cx62, in human and mouse (Cx57, mouse homologue) platelets. A novel mimetic peptide (^{62}Gap27) was developed to target the second extracellular loop of Cx62 and 3D structural models predicted its interference with gap junction and hemichannel function. The ability of ^{62}Gap27 to regulate both gap junction and hemichannel-mediated intercellular communication was observed using FRAP analysis and flow cytometry. Cx62 inhibition by ^{62}Gap27 suppressed a range of agonist-stimulated platelet functions and impaired thrombosis and haemostasis. This was associated with elevated PKA-dependent signalling in a cyclic adenosine monophosphate-independent manner, and was not observed in Cx57 deficient mouse platelets (in which the selectivity of ^{62}Gap27 for this connexin was also confirmed). Notably, Cx62 hemichannels were observed to function independently of Cx37 and Cx40 hemichannels. Together, our data reveal a fundamental role for a hitherto uncharacterised connexin in the regulation of the function of circulating cells.

Introduction

Connexins (Cxs) constitute a family of channel-forming proteins that are distributed widely in different cell types.[1-3] Connexins oligomerize in the endoplasmic reticulum to form 6-membered structures known as hemichannels that are transported to the plasma membrane. Hemichannels on adjacent cells dock together to form gap junctions or pore-like structures (~2-3 nm) that facilitate contact-dependent inter-cellular trafficking of small molecules (up to 1 kDa) between adjacent cells, enabling coordinated cellular responses.[1,4].

Gap Junctions and hemichannels have been studied in various cell types, where they mediate stable cellular interactions and through mediation of intercellular signalling coordinate synchronised cell function within tissues.[5] The cardiovascular functions of connexins are well-characterised, from cardiac myocyte contraction[6-8] to control of vascular function.[9-11] Notably, connexins such as Cx37, Cx40 and Cx43, present in the vasculature, have been reported to contribute to the development of atherosclerosis[12-14], a process in which circulating inflammatory cells are implicated.[15-17] The reported roles of connexins in regulating the activities of immune cells including monocytes, macrophages, T cells, and dendritic cells, in addition to platelets, are therefore particularly pertinent.[18-21]

Platelets are regulators of hemostasis and aggregate at sites of vascular damage to form thrombi that prevent excessive loss of blood.[22,23] Increasing evidence indicates the importance of sustained signaling between platelets within a thrombus, to ensure thrombus growth and stability, and the importance of direct intercellular communication between adjacent platelets.[24,25]

We have reported the presence of Cx37 and Cx40 in platelets and through the use of selective mimetic peptides and transgenic gene-deficient mice, demonstrated that both hemichannels and gap junctions are required for platelet activation and thrombus formation.[26,27] In addition to Cx37 and Cx40, we observed notable levels of Cx62 mRNA transcripts in megakaryocytes and circulating cells such as B-cells, T-cells and monocytes.[26] Very little is known regarding the properties, function and tissue distribution of this 'orphan' connexin, which has previously only been reported to be expressed in mouse (the mouse homolog is Cx57), in retina and muscle cells.[28,29] Given this, we explored whether Cx62 has a role in platelets.

Using a newly designed inhibitory peptide (^{62}Gap27) and Cx57-deficient mice, we reveal the importance of Cx62(57) for the regulation of intercellular signaling in platelets and within thrombi. Furthermore, we demonstrate that ^{62}Gap27 inhibits platelet function by stimulating PKA-mediated inhibitory signaling that protects mice from thrombosis.

Methods

The preparation of washed platelets, immunoblotting, immunofluorescence, and platelet functional assays such as aggregation, dense granule secretion, fibrinogen binding, P-selectin exposure, calcium mobilization, clot retraction, platelet spreading, thrombus formation, and tail bleeding was performed as described previously.[26,27,30-32] Detailed descriptions of reagents and these methods are provided in Supplemental Methods.

Mice

Gja10$^{em2(IMPC)Mbp}$ mice were produced by insertion of an indel-causing frameshift mutation by the International Mouse Phenotyping Consortium (IMPC) at the University of California, Davis, and mice obtained in collaboration with the Mary Lyon Centre,

Harwell, UK. Phenotyping of these mice in the IMPC pipeline revealed normal blood count parameters. C57BL/6 mice were purchased from Envigo (Huntingdon, UK).

Statistical analysis

Data were analysed using student T-test and if more than two means were present, significance was determined by one way ANOVA, Two-way ANOVA (*in vitro* thrombus formation assay), Nonparametric Mann–Whitney U-test (*in vivo* thrombosis and amount of blood loss in tail-bleeding assay) and Fisher's Exact test (time to cessation of bleeding in tail bleeding assay). Data represent mean ± SD and $P < 0.05$ was considered to be statistically significant. Statistical analysis was performed using GraphPad Prism 7.0 software (California, USA).

Results

Expression of Connexin 62 in Platelets

The expression of Cx62 in human platelets and the megakaryocytic cell line MegO1 was confirmed using immunoblot analysis and the expression of Cx57 in mouse platelets was also observed (Figure 1A). HeLa cells are devoid of other connexin family members[33] and were confirmed not to express detectable levels of Cx62. Immunofluorescence studies performed on resting permeabilized human platelets revealed Cx62 (stained red) to be present in a punctate arrangement inside platelets (stained green for GPIb) and were redistributed towards the periphery of the cells upon activation with the TxA_2 mimetic peptide U46619 (used at a concentration at which platelet shape-change is minimal) (Figure 1B-C).

We also utilized super-resolution STORM microscopy to determine the subcellular localization of Cx62. In comparison to the resting platelets, Cx62 (stained red) redistributed on (or near) to the plasma membrane (stained green for integrin β3) and

appeared to be arranged in clusters, thereby, increasing proximity to integrin β3 in the plasma membrane (Figure 1D). Treatment with secondary antibody alone (in the absence of Cx62 primary antibody) was performed to exclude the possibility of non-specific staining (Supplemental figure 1A). To further confirm the translocation of Cx62 to the plasma membrane upon platelet activation, co-localization of integrin β3 subunit and Cx62 in resting and thrombin-stimulated platelets was analyzed using the coordinate-based colocalization (CBC) method.[34] In CBC analysis, each molecule is assigned a value between -1 and 1. CBC values of zero indicate a homogeneous distribution of molecules and positive values indicate increasing localization of the two sets of molecules. The shift in the CBC curve to predominantly positive values upon platelet stimulation, therefore, indicates increased colocalization (Figure 1E). In non-stimulated platelets, approximately 20% of the Cx62 population co-localized with integrin β3, which increased to approximately 85% upon platelet activation (5 minutes) (Figure 1E).

To further explore the subcellular-location of Cx62 in platelets, we performed a linear sucrose density gradient centrifugation on platelet homogenates, following nitrogen cavitation. Cx62 was highly concentrated in the low-density fractions (1 and 2) with a distribution profile similar to that of calreticulin [a marker of the dense tubular system (DTS)] and β3 integrin but was absent from higher density fractions (9 and 10), where α-granule cargo such as TSP-1 was present (Supplemental figure 1B). These data are consistent with the presence of Cx62 inside and on the surface of platelets, and further recruitment to the cell surface during platelet activation.

Cx62 Structural Prediction

To assist in the design and analysis of an inhibitory mimetic peptide that specifically targets Cx62(57), the monomeric and oligomeric structures of Cx62 were predicted. The

predicted tertiary structure of Cx62 from the IntFOLD server[35] reveals a protomer (monomer subunit) consisting of four transmembrane helices, two extracellular loops, a small bended N-terminal helix, and a long disordered cytoplasmic C-terminus loop (Figure 2A-B). The ModFOLD6[36] global 3D model quality score for the full-length protein was calculated as 0.43 ($p < 0.01$; less than a 1 in 100 chance of being incorrect), which increased to 0.57 ($p<0.001$; less than a 1 in 1000 chance of being incorrect) when the long-disordered C-terminal loop was excluded. The calculated local (or per-residue) errors indicate that the ordered regions of the Cx62 structure were modelled with high confidence (Figure 2A). The tertiary structure model of Cx62 was subsequently used as a target for *in silico* docking with the designed mimetic peptide, and for quaternary structure assembly of the docked hemichannel complex (Figure 2C-E).

Design of the Cx62 Mimetic Peptide (^{62}Gap27) and Protein-Ligand Docking Studies

Due to the lack of an existing Cx62 selective inhibitor, we designed a mimetic peptide (^{62}Gap27) that targets the second external loop of Cx62(57). To confirm the molecular interactions between Cx62 and ^{62}Gap27, single ligand docking prediction was performed using SwissDock. Six of the clusters from SwissDock contained alternative ligand poses that were bound in approximately the same location at the end of the second external loop (Figure 2B) (Supplemental figure 1D).

Cx62 Forms Hemichannels and Gap Junctions in Platelets

The exact mode of action by which different Gap27 peptides function is not clearly understood. It is believed that they induce a conformational change in the hemichannel, that prevents them from docking to form a gap junction and thus modulate the permeability of the pore.[21,26,37,38] To investigate this, we performed flow cytometry using calcein-loaded human platelets, where efflux of calcein from the platelet cytosol was

measured to determine the effect of ^{62}Gap27 on Cx62 permeability (Figure 2F-G). Upon thrombin stimulation (0.1 U/ml), calcein-associated fluorescence decreased in scrambled peptide-treated cells by approximately 50%, indicating a release of dye. The treatment of platelets with ^{62}Gap27 (100 μg/ml) prevented this loss of fluorescence. Since flow cytometry-based analyses involve the gating of individual platelets, this indicates a role for Cx62 hemichannels in regulating platelet permeability. Given the strong reduction in the level of calecin efflux observed in ^{62}Gap27-treated platelets, it is plausible that the peptide not only blocks Cx62 function but also inhibits the function of heteromers formed by Cx62 with other connexin isoforms present on platelets (e.g. Cx37and Cx40). At the same thrombin concentration, ^{62}Gap27 did not reduce the extent of P-selectin exposure (a marker of α-granule secretion) on the platelet surface, in comparison to scrambled peptide treatment (Supplemental figure 1C). This suggests that the effects of ^{62}Gap27 observed on the permeability of hemichannels were not due to a reduction in the activation state of platelets under these experimental conditions.

To evaluate the ability of ^{62}Gap27 to modulate gap junction-mediated intercellular communication, fluorescence recovery after photobleaching (FRAP) analysis was performed. Calcein-labeled platelets were incubated on coverslips coated with fibrinogen and collagen together (to ensure maximal platelet adhesion and spreading) and a defined region of cells was bleached by laser-exposure. Fluorescence recovery in ^{62}Gap27-treated platelet aggregates was halved in comparison to scrambled peptide-treated samples (17%) (Figure 2H-I). These findings demonstrate gap junction-mediated intercellular communication between platelets and the inhibitory effect of ^{62}Gap27 on this.

The model of the Cx62 hemichannel complex (Figure 2C-D) revealed the two interacting hemichannels forming the putative structure of the Cx62 gap junction channel (Figure

2E). In the close-up view of the interface, the residues mediating the inter-hemichannel interactions are shown to be present in the first and second external loops (Figure 2E). Protomer-inhibitor (Cx62-^{62}Gap27) interface residues were not found to coincide with the interface residues of the 12-mer (docked-hemichannel). Additionally, there are no SwissDock poses within the most common ^{62}Gap27 inhibitor interaction location (Figure 2D) that share any interface residues with the with 6-mer (hemichannel) assembly (Figure 2D). Therefore, the inhibitor binding at this site is unlikely to disrupt either the assembly of the 6-mer or the hemichannel-hemichannel complex (12-mer) (Figure 2E).

The predicted ^{62}Gap27 binding site was shown to coincide with the subsequent residues from which the inhibitor was designed from (203-213, SRPTEKTIFML) (Figure 2B-C). Specifically, the inhibitor is likely to bind to both T209 and L213 (bold circles Figure 2B). The additional interaction of the inhibitor with residues in the loop regions from 180-183 (GFQM) suggests a potential mechanism for the regulation of flow through the pore. The interaction may act to decrease the flexibility in the loop regions of the hemichannel pore, thereby regulating permeability (Figure 2C-D).

^{62}Gap27 Negatively Regulates Platelet Aggregation and Integrin Activation

Light transmission aggregometry was used to investigate the effects of ^{62}Gap27 on human washed platelets stimulated with a range of platelet activators that target different receptors. The concentrations of platelet agonists used were optimized for each donor to attain 50% maximal aggregation (EC_{50}) following 3 minutes of stimulation. Pre-treatment of platelets with ^{62}Gap27 (50 and 100 μg/ml) for 5 minutes caused a concentration-dependent inhibition to both CRP-XL (GPVI receptor-specific platelet agonist; EC_{50}: 0.2 - 0.4 μg/ml) and thrombin (EC_{50}: 0.05 – 0.08 U/ml) mediated platelet aggregation (Figure 3A-B). The scrambled peptide (100 μg/ml) was without effect (Supplemental figure 2A).

Inhibition of approximately 45% (50 μg/ml ^{62}Gap27) and 65% (100 μg/ml ^{62}Gap27) was observed against CRP-XL and thrombin-stimulated aggregation respectively. ^{62}Gap27 also attenuated platelet aggregation stimulated by U46619 (EC_{50}: 0.25 - 0.4 μM) (Supplemental figure 2B) and ADP (EC_{50}: 5-10 μM) (Supplemental figure 2C). These data suggest that the effects of ^{62}Gap27 and therefore Cx62 functions are common to a variety of platelet agonists.

Flow cytometry was used to measure the level of fibrinogen binding to activated integrin αIIbβ3. Consistent with reduced aggregation, CRP-XL or thrombin-stimulated fibrinogen binding was reduced by 55% and 65% respectively, following ^{62}Gap27 (100 μg/ml) treatment (Figure 3C). The scrambled peptide was without effect (Supplemental figure 2D). Since fibrinogen binding was measured on gated single platelets, this provides additional evidence that Cx62 hemichannels participate in the initiation of platelet activation.

The actions of ^{62}Gap27 are mediated selectively via Cx62

To confirm the selectivity of ^{62}Gap27 mimetic peptide towards Cx62(57), its effects were examined in Cx57$^{-/-}$ platelets. The deletion of Cx57 did not alter the expression of other platelet connexins such as Cx37 and Cx40 (Supplemental figure 3A-B). Similarly, the deletion of Cx37 and Cx40 did not affect the expression of Cx57 (Supplemental figure 3C-D). The expression of GPVI, integrin α2β1, integrin αIIbβ3 and GPIb on the surface of Cx57$^{+/+}$ and Cx57$^{-/-}$ platelets was not significantly different (Supplemental figure 3E-H).

In comparison with scrambled peptide, treatment with ^{62}Gap27 (100 μg/ml) inhibited CRP-XL-mediated fibrinogen binding in Cx57$^{+/+}$ platelets (in PRP) but was without effect on Cx57$^{-/-}$ platelets (Figure 3D), confirming the specificity of ^{62}Gap27 for Cx57, which in turn signifies its selectivity for Cx62 in humans. Additionally, ^{37,43}Gap27 and ^{40}Gap27

treatment (mimetic peptides for Cx37 and Cx40, respectively) significantly inhibited fibrinogen binding in both $Cx57^{+/+}$ and $Cx57^{-/-}$ platelets (Figure 3D). Consistent with this, ^{62}Gap27 also inhibited CRP-XL-stimulated fibrinogen binding in $Cx37^{-/-}$ and $Cx40^{-/-}$ platelets to a similar extent as in littermate $Cx37^{+/+}$ and $Cx40^{+/+}$ platelets (Supplemental Figure 4A-B). This suggests that Cx37, Cx40 and Cx57 hemichannels can function independently of each other in platelets and the deletion of one connexin does not affect the functions of other platelet connexins. Furthermore, a significant reduction in fibrinogen binding was observed in CRP-XL-stimulated $Cx57^{-/-}$ platelets, in comparison to $Cx57^{+/+}$ platelets. This indicates a fundamental role of Cx57 in regulating platelet activation (Figure 3E).

^{62}Gap27 Inhibits Platelet Secretion

To assess the effects of ^{62}Gap27 on platelet secretion, P-selectin surface exposure and ATP release (a marker of dense granule secretion) were evaluated using flow cytometry and luciferin-luciferase luminescence assay, respectively. Incubation of platelets (in PRP) with ^{62}Gap27 attenuated (in comparison to scrambled peptide) P-selectin exposure, reaching 60% inhibition (at 100 μg/ml ^{62}Gap27) upon stimulation with CRP-XL or thrombin (Figure 3F). Scrambled peptide (100 μg/ml) was without effect (Supplemental Figure 4C). CRP-XL or thrombin-stimulated ATP release was also attenuated by approximately 65% and 50% respectively upon treatment with ^{62}Gap27 (100 μg/ml), in comparison to the scrambled peptide (Figure 3G).

Activated platelets synthesize TxA_2 to provide positive feedback, enabling the recruitment of more platelets to the hemostatic plug.[39] Treatment of washed platelets with ^{62}Gap27 attenuated both CRP-XL or thrombin stimulated production of TxB_2 (a stable metabolite of TxA_2) (Figure 3H).

Integrin-mediated platelet adhesion and signaling is regulated by Cx62

Binding of fibrinogen to integrin αIIbβ3 initiates integrin clustering and outside-in signaling that reinforces platelet activation and ensures the stability of thrombus.[40] Platelet spreading and clot-retraction are direct outcomes of outside-in signaling.[41] The effects of ^{62}Gap27 on platelet adhesion and spreading on fibrinogen coated-coverslips were investigated. In comparison with the scrambled peptide-treated controls, ^{62}Gap27 (50 and 100 μg/ml) significantly reduced platelet adhesion to fibrinogen (Figure 4A). The proportion of adhered platelets reaching lamellipodia stage was also down-regulated by ^{62}Gap27 (Figure 4A). In the absence of agonist pre-stimulation, the ability of ^{62}Gap27 to attenuate platelet adhesion to fibrinogen-coated coverslips suggests underlying levels of platelet signaling that are associated with Cx62 function and can modulate integrin affinity and fibrinogen binding. Consistent with this, fibrin clot retraction was also inhibited, indicating the role of Cx62 in the formation and consolidation of thrombi (Figure 4B).

Cx62(57) Modulates Thrombosis and Haemostasis

To elucidate the function of Cx62 in platelets under shear in whole blood, we determined the effects of ^{62}Gap27 on thrombus formation *in vitro* using fluorescence microscopy. $DiOC_6$-labelled whole human blood, treated with scrambled peptide or ^{62}Gap27 (100μg/ml), was perfused through collagen-coated microfluidic flow channels for 10 minutes at a shear rate of 500 s^{-1} (20 dyn/cm^2). The mean fluorescence intensity of thrombi in ^{62}Gap27-treated whole-blood was reduced by 70%, in comparison with scrambled peptide (Figure 4C). Furthermore, the extent of thrombus surface coverage was also attenuated in ^{62}Gap27-treated samples, consistent with impaired adhesion of platelets (Supplemental Figure 4D).

The acute effects of ^{62}Gap27 (100 μg/ml) on thrombosis was investigated in mice following laser-induced injury of cremaster muscle arterioles and observed using intravital microscopy. Large and stable thrombi were formed in scrambled peptide-treated mice, whereas, ^{62}Gap27 treatment resulted in the development of substantially smaller thrombi that were unstable and embolized, resulting in a three-fold reduction in the mean of maximum fluorescence intensity (Figure 4D-E).

The contribution of Cx57(62) to haemostasis was assessed by measuring tail-bleeding time. While bleeding stopped in all 9 scrambled peptide-treated mice (mean bleeding time, 459 ± 81 seconds), the time to cessation of bleeding was dramatically increased in ^{62}Gap27-treated mice where 7 of 10 mice bled for more than 20 minutes (Figure 4F). In alignment with this, the amount of blood loss in ^{62}Gap27-treated mice was higher than the scrambled peptide-treated mice, indicating impaired hemostasis (Figure 4G).

^{62}Gap27 negatively regulates GPVI and thrombin-mediated signaling in platelets

Given the effects of ^{62}Gap27 on CRP-XL-mediated platelet responses and thrombus formation *in vitro* and *in viv*o, we investigated the effects of ^{62}Gap27 on signal transduction stimulated by the GPVI receptor. Pre-treatment of platelets (non-aggregation conditions) with ^{62}Gap27 (50 and 100 μg/mL) for 5 minutes reduced CRP-XL-stimulated total protein tyrosine phosphorylation by approximately 25% and 30% respectively, in comparison with scrambled peptide (Figure 5A). Consistent with this, 100 μg/ml of ^{62}Gap27 inhibited the tyrosine phosphorylation of Syk (Tyr$^{525/526}$) by ~30% (Figure 5B). This indicated that ^{62}Gap27 inhibits the early stages of the GPVI signaling. Activated Syk results in phosphorylation of the transmembrane adapter protein LAT, followed with PLCγ2 phosphorylation.[41] Tyrosine phosphorylation of LAT (Tyr^{200}) and

PLCγ2 (Tyr^{1217}) were observed to be diminished by 40% and 25% respectively, following ^{62}Gap27 treatment (100 μg/ml) compared to the scrambled peptide (Figure 5C-D).

Downstream of PLCγ2, ^{62}Gap27 inhibited CRP-XL-stimulated (0.25 μg/ml) calcium mobilization by 45%, when compared with scrambled peptide (Figure 5E). Treatment with saturating concentrations of EGTA (2 mM) to prevent Ca^{2+} influx, in the presence of scrambled peptide, reduced CRP-XL-mediated rise in cytosolic calcium concentration by approximately 50%, in comparison to scrambled peptide alone. The inhibitory effects of ^{62}Gap27 (100 μg/ml) were found to be additive to the reduction caused by EGTA-scrambled peptide, following stimulation with CRP-XL (0.5 μg/ml) (Supplemental figure 5A), suggesting that Cx62 can modulate the release of calcium from intracellular stores. Consistent with this, CRP-XL evoked PKC substrate phosphorylation was also found to be attenuated by 45% (Figure 5F), following incubation with ^{62}Gap27 (100 μg/ml). Furthermore, ^{62}Gap27 also reduced ERK1/2 phosphorylation in CRP-XL stimulated platelets, which is consistent with the down-regulation of CRP-XL evoked TxA_2 (TxB_2) release (Supplemental Figure 5F). Similar inhibition was observed following ^{37,43}Gap27 treatment (Supplemental Figure 5F).

In comparison with scrambled peptide, ^{62}Gap27 also inhibited thrombin-evoked total protein tyrosine phosphorylation, calcium mobilization, the release of calcium from intracellular stores, PKC substrate phosphorylation and ERK1/2 phosphorylation (Supplemental Figure 5B-F).

To confirm that signaling events following GPVI activation were affected by Cx57 in mice, GPVI signaling events were investigated in Cx57$^{+/+}$ and Cx57$^{-/-}$ platelets. Cx57-deficient platelets showed reduced CRP-XL-evoked total tyrosine phosphorylation and phosphorylation of Syk (Tyr$^{525/526}$), LAT (Tyr^{200}), PLCγ2 (Tyr^{1217}) and PKC substrates in

comparison with $Cx57^{+/+}$ mouse platelets (Figure 6A-E), suggesting the importance of Cx57 in GPVI signaling.

^{62}Gap27 activates PKA independently of cyclic nucleotide signaling

The effects of ^{62}Gap27 on GPVI-specific signaling events were surprising given the ability of the peptide to inhibit platelet responses to several agonists including thrombin, which would suggest a mechanism that would be common to each. Platelets are maintained in a quiescent state by prostaglandin I_2 (PGI_2) and nitric oxide (NO), released by endothelial cells.[42,43] PGI_2 binds to IP receptor and stimulates the production of cyclic adenosine monophosphate (cAMP), while NO stimulates the production of cyclic guanosine monophosphate (cGMP) which activate protein kinase A (PKA) and protein kinase G (PKG), respectively, and inhibit platelet activation through phosphorylation of multiple substrates.[44,45]

We therefore explored the effect of ^{62}Gap27 on PKA and PKG-dependent signaling in platelets by measuring the extent of VASP (Vasodilator-stimulated phosphoprotein) phosphorylation at Ser^{157} and Ser^{239} respectively (PKA- and PKG-selective phosphorylation sites). The treatment of resting platelets with ^{62}Gap27 upregulated the phosphorylation of VASP S^{157} in comparison with scrambled peptide (Figure 7A), while no effect on VASP S^{239} was observed (Supplemental figure 6A). VASP S^{157} phosphorylation was also elevated in CRP-XL-stimulated platelets that were treated with ^{62}Gap27 in comparison with scrambled peptide-treated control (Figure 7B). Additionally, we observed that resting platelets when treated with ^{37,43}Gap27 also upregulate VASP S^{157} phosphorylation in comparison with scrambled peptide (Supplemental figure 6B). This suggests that activation of PKA represents a general mechanism by which Gap27 peptides inhibit platelet functions.

VASP phosphorylation was reversed following treatment with PKA inhibitors; H89 (10 μM) (Figure 7C) or PKI (10 μM) (Figure 7D), confirming a key role for PKA in this process. We examined cAMP concentration in resting and CRP-XL activated platelets treated with ^{62}Gap27 (100μg/ml) or scrambled peptide. Treatment with ^{62}Gap27 did not elevate cAMP levels in resting or CRP-XL-stimulated platelets (Figure 7E). Similarly, ^{62}Gap27 did not up-regulate cAMP concentration in thrombin-stimulated platelets (Supplemental figure 6C). In agreement with this, ^{62}Gap27-stimulated VASP phosphorylation was not reduced by treatment with, Rp-8-CPT-cAMPs (200 μM) (Figure 7F), a competitive inhibitor of cAMP-binding to PKA or the adenylyl cyclase inhibitor SQ22536 (100 μM) (Figure 7G). Together these data indicate that ^{62}Gap27 inhibits platelet function through activation of PKA, independently of cAMP.

S^{157} VASP phosphorylation was also investigated in Cx57$^{+/+}$ and Cx57$^{-/-}$ mouse platelets in the presence and absence of PKA inhibitors. Consistent with observations on human platelets, ^{62}Gap27-treated Cx57$^{+/+}$ mouse platelets exhibited enhanced VASP S^{157} phosphorylation, in comparison to scrambled peptide-treated samples, which was reversed upon treatment with the PKA inhibitor H89 (Figure 7H) but not reversed by Rp-8-CPT-cAMPs (Figure 7I). ^{62}Gap27 treatment of Cx57$^{-/-}$ mouse platelets did not result in VASP phosphorylation, further confirming the specificity of action of ^{62}Gap27 (Figure 7H, 7J).

It has been reported that PKC isoforms, PI3-Kinase or PKB/Akt can contribute towards the phosphorylation of VASP.[32,46,47] However, ^{62}Gap27 induced VASP phosphorylation in platelets was not prevented upon treatment with either a pan-PKC inhibitor GF109203X (10 μM), PI3-Kinase inhibitor LY29400 (100 μM) or AKT inhibitor IV (5 μM) (Supplemental figure 6D-F). Together, these observations provide insight into the

mechanism through which the actions of ^{62}Gap27 on Cx62 inhibit platelet activation through the up-regulation of PKA activity independently of cAMP.

Discussion

Growing evidence suggests the role of different platelet surface receptors (Eph kinase, CD72, plexin-B1 and CD40L) in contact-dependent signaling that is required for the formation of a stable thrombus.[48,49] The contributions of gap junction-mediated intercellular communication to platelet function and thrombus growth represents a recently discovered paradigm for the regulation of circulating cells following cell-cell contact. In this study, we describe the presence of Cx62(57) in platelets, which was found in a punctate arrangement in the cytosol and translocated to the plasma membrane upon activation. These observations are consistent with the formation of hemichannels on the cell membrane, and the formation of gap junctions as adjacent platelets make sustained contact within a thrombus. The mechanism by which Cx62 traffics to the cell membrane upon platelet activation remains to be established. In other cell types, connexins translocate to the plasma membrane through the classical secretory pathway.[50-54] In platelets, Cx62 is distributed similarly to calreticulin, present within the DTS (remnants of megakaryocyte smooth endoplasmic reticulum) but not in subcellular fractions that contain α-granule cargo or cytosolic proteins, suggesting a non-classical secretion mechanism. It has been proposed that connexins are chaperoned by protein disulfide-isomerases, as connexin extracellular loops are exposed in the endoplasmic reticulum to form disulfide bonds.[55] Protein disulfide-isomerases also localize to the platelet DTS and become mobilized in activated platelets, and therefore may share mechanisms of trafficking towards the cell surface with Cx62.[56]

To determine the role of Cx62 in the regulation of platelet function, a novel synthetic mimetic peptide (^{62}Gap27) targeting Cx62(57) was designed. Its inability to inhibit CRP-XL-mediated fibrinogen binding in Cx57$^{-/-}$ mice, in comparison to Cx57$^{+/+}$ confirmed its selective action towards Cx57/62. Incubation with ^{62}Gap27 significantly down-regulated calcein release from activated platelets in suspension (non-aggregated), which points towards a role for connexin hemichannels in the early phases of platelet activation. This was associated with diminished markers of platelet activation such as fibrinogen binding, and dense- (ATP-release) and α-granule (P-selectin exposure) secretion. It is interesting to note that pannexin-1 releases cytosolic ATP, which primes platelet responses when exposed to low agonist concentrations via the effect of the ATP on P2X1 channels.[57] The possibility that direct release of ATP represents a mechanism through which connexins contribute to platelet activation is a priority for investigation in future work. Additionally, FRAP experiments confirmed the formation of Cx62-containing gap junctions between adjacent platelets. Thrombus stability was suppressed both *in vitro* and *in vivo* following treatment with ^{62}Gap27, indicating the vital role of gap junction intercellular communication in the reinforcement of thrombi. It is plausible that such robust effects of ^{62}Gap27 on thrombosis *in vivo* are partly due to its effects on other circulating or endothelial cells. Further work to explore this will require transgenic mice with platelet-specific deletion of Cx57.

Studies in Cx57-deficient mouse platelets identified that Cx57(62) positively regulates platelet function, hemostasis and thrombus formation. These functions are shared with Cx37 and Cx40, the other principal platelet connexins.[21,26,27,58] We also observed negative regulation of Ca^{2+} mobilization following treatment with ^{62}Gap27. This inhibition was identified to be partly due to reduced Ca^{2+} mobilization from stores, although effects on

the Ca^{2+} influx cannot be ruled out. Numerous channels regulate calcium mobilization in platelets, including P2X1, TRPC6, STIM1 and Orai1.[41,42,59] Notably Cx43 has been shown to interact with the calcium channel P2X1.[60] It is therefore possible that Cx62 may associate with a platelet calcium channel to influence calcium mobilization.

PKA activation plays an essential role in the regulation of platelet function by controlling several aspects of activation including integrin αIIbβ3 affinity, inositol 1,4,5-trisphosphate (IP_3) receptor function and shape change via actin polymerisation.[61,62] While cAMP is a key activator of PKA in platelets, studies have also reported that PKA activity can be stimulated by collagen or thrombin in a cAMP-independent manner, and in other cells, cAMP-independent PKA activation has been attributed to the effects of sphingosine and free radicals.[47,63-65] We provide compelling evidence that the inhibitory effects of ^{62}Gap27 on platelets are mediated through increased PKA activity, independently of cAMP. Notably, cAMP-independent upregulation of PKA signalling occurs in unstimulated platelets which suggest a direct influence of ^{62}Gap27 binding to Cx62 on PKA activity. The mechanism by which ^{62}Gap27 induces PKA activation remains unclear. Since ^{62}Gap27 is predicted to primarily induce conformational changes in Cx62 (Figure 2C and Supplemental figure 1D), we speculate that ^{62}Gap27 binding may influence the ability of PKA to interact with the connexin, or localized A-kinase anchoring proteins (AKAPs) that may modulate PKA activity in the vicinity of the connexin. The lack of increased VASP phosphorylation in Cx57-deficient platelets in the absence of ^{62}Gap27 suggests that Cx binding of PKA may result in its activation, while non-Cx57-bound PKA is inactive.

It is possible that connexin-associated PKA may be responsible for the regulation of connexin trafficking (noting that platelet activation results in recruitment to the plasma

membrane) or regulation of channel function. Further work will be required to determine the precise mechanism of PKA activation in the presence or absence of ^{62}Gap27 to assess whether this represents conformational perturbation of Cx62 by the peptide or involves PKA-mediated phosphorylation of the connexin that modulates channel activity. Notably the absence of Cx57, which in itself does not alter PKA-dependent signalling in unstimulated platelets, results in diminished levels of platelet activation. This supports a role for Cx57 channel activity in the function of platelets. It remains to be established whether the inhibitory effects of ^{62}Gap27 are solely mediated through stimulation of PKA signalling (which is dependent on the presence of the connexin) or also through modulation of channel function. It is pertinent that several studies indicate the involvement of PKA and PKG in regulating the phosphorylation of Cx32, Cx35/36, Cx40, Cx43 and Cx50 in various cell types.[66-71] In the absence of antibodies that allow the immunoprecipitation of Cx62, we have, thus far, been unable to determine whether Cx62 represents a PKA substrate in platelets.

The potential link between Cx62 and thrombotic disease risk is uncertain, and relevant mutations that might modulate such risk have not been identified. The expression of Cx62 is not widespread which may enhance its potential as a therapeutic target, minimising side-effects, noting that systemic genetic deletion of Cx57 in mice is well-tolerated. Our Gap27 peptide docking experiments are suggestive of regulation of gating by conformational changes, although, as discussed, modulation of PKA-dependent signaling may also be important. Non-peptide based selective inhibitors would need to be developed that potentially mimic peptide binding and/or associated conformational changes in order to develop this further. A suggested starting point for such work would

be the development of biologics that target the proposed ^{62}Gap27 binding sequences predicted in Cx62.

In summary, we have identified key functions for the orphan connexin, Cx62(57) in platelets in the regulation of hemostasis and thrombosis. We have revealed a new signaling mechanism through which Cx62(57) and its inhibitor modulate cellular function and highlight the importance of connexin hemichannels and gap junctions in the regulation of the function of circulating cells.

Acknowledgments

This work was supported by the Saudi Cultural Bureau (London), a Felix Scholarship (2014-17), grants from the British Heart Foundation (RG/09/011/28094 and RG/15/2/31224), the Medical Research Council (MR/J002666/1 and MR/P023878/1), and the Biotechnology and Biological Sciences Research Council.

Authorship

K.A.S. and G.D.F. designed the research, performed experiments, analysed results, and wrote the article. P.S., A.H.M., L.M.H., S.K.A and A.E. performed experiments and analysed results. T.S., A.R.S., R.A., M.A., M.C., A.P.B., NK, SV, A.J.U and C.I.J performed experiments. L.J.M. and J.M.G. designed the research, analysed data and wrote the article.

Footnotes

*KAS and GDF are joint first authors.

Conflict-of-interest disclosure: The authors declare no competing financial interests.

References

1. Batra N, Kar R, Jiang JX. Gap Junctions and Hemichannels in Signal Transmission, Function and Development of Bone. *Biochimica et biophysica acta*. 2012;1818(8):1909-1918.

2. Goodenough DA, Paul DL. Gap junctions. *Cold Spring Harb Perspect Biol*. 2009;1(1):a002576.
3. Hanner F, Sorensen CM, Holstein-Rathlou N-H, Peti-Peterdi J. Connexins and the kidney. *American Journal of Physiology-Regulatory, Integrative and Comparative Physiology*. 2010;298(5):R1143-R1155.
4. Koval M, Molina SA, Burt JM. Mix and match: investigating heteromeric and heterotypic gap junction channels in model systems and native tissues. *FEBS letters*. 2014;588(8):1193-1204.
5. Huettner JE, Lu A, Qu Y, Wu Y, Kim M, McDonald JW. Gap junctions and connexon hemichannels in human embryonic stem cells. *Stem Cells*. 2006;24(7):1654-1667.
6. Kostin S, Dammer S, Hein S, Klovekorn WP, Bauer EP, Schaper J. Connexin 43 expression and distribution in compensated and decompensated cardiac hypertrophy in patients with aortic stenosis. *Cardiovasc Res*. 2004;62(2):426-436.
7. Darrow BJ, Fast VG, Kléber AG, Beyer EC, Saffitz JE. Functional and structural assessment of intercellular communication. Increased conduction velocity and enhanced connexin expression in dibutyryl cAMP-treated cultured cardiac myocytes. *Circ Res*. 1996;79(2):174-183.
8. Oyamada M, Kimura H, Oyamada Y, Miyamoto A, Ohshika H, Mori M. The expression, phosphorylation, and localization of connexin 43 and gap-junctional intercellular communication during the establishment of a synchronized contraction of cultured neonatal rat cardiac myocytes. *Exp Cell Res*. 1994;212(2):351-358.
9. Molica F, Figueroa XF, Kwak BR, Isakson BE, Gibbins JM. Connexins and Pannexins in Vascular Function and Disease. *Int J Mol Sci*. 2018;19(6).
10. Figueroa XF, Isakson BE, Duling BR. Connexins: gaps in our knowledge of vascular function. *Physiology (Bethesda)*. 2004;19:277-284.
11. Billaud M, Lohman AW, Johnstone SR, Biwer LA, Mutchler S, Isakson BE. Regulation of cellular communication by signaling microdomains in the blood vessel wall. *Pharmacological reviews*. 2014;66(2):513-569.
12. Kwak BR, Mulhaupt F, Veillard N, Gros DB, Mach F. Altered pattern of vascular connexin expression in atherosclerotic plaques. *Arterioscler Thromb Vasc Biol*. 2002;22(2):225-230.
13. Johnstone SR, Ross J, Rizzo MJ, et al. Oxidized phospholipid species promote in vivo differential cx43 phosphorylation and vascular smooth muscle cell proliferation. *The American journal of pathology*. 2009;175(2):916-924.
14. Yeh HI, Lu CS, Wu YJ, et al. Reduced expression of endothelial connexin37 and connexin40 in hyperlipidemic mice: recovery of connexin37 after 7-day simvastatin treatment. *Arterioscler Thromb Vasc Biol*. 2003;23(8):1391-1397.
15. Ilhan F, Kalkanli ST. Atherosclerosis and the role of immune cells. *World journal of clinical cases*. 2015;3(4):345-352.
16. Ammirati E, Moroni F, Magnoni M, Camici PG. The role of T and B cells in human atherosclerosis and atherothrombosis. *Clinical and experimental immunology*. 2015;179(2):173-187.
17. Hartwig H, Silvestre Roig C, Daemen M, Lutgens E, Soehnlein O. Neutrophils in atherosclerosis. A brief overview. *Hamostaseologie*. 2015;35(2):121-127.
18. Anand RJ, Dai S, Gribar SC, et al. A role for connexin43 in macrophage phagocytosis and host survival after bacterial peritoneal infection. *J Immunol*. 2008;181(12):8534-8543.
19. Sarieddine MZ, Scheckenbach KE, Foglia B, et al. Connexin43 modulates neutrophil recruitment to the lung. *J Cell Mol Med*. 2009;13(11-12):4560-4570.
20. Machtaler S, Dang-Lawson M, Choi K, Jang C, Naus CC, Matsuuchi L. The gap junction protein Cx43 regulates B-lymphocyte spreading and adhesion. *Journal of cell science*. 2011;124(15):2611-2621.
21. Vaiyapuri S, Flora GD, Gibbins JM. Gap junctions and connexin hemichannels in the regulation of haemostasis and thrombosis. *Biochem Soc Trans*. 2015;43(3):489-494.
22. Badimon L, Padró T, Vilahur G. Atherosclerosis, platelets and thrombosis in acute ischaemic heart disease. *European Heart Journal: Acute Cardiovascular Care*. 2012;1(1):60-74.
23. Flora GD, Nayak MK. A Brief Review of Cardiovascular Diseases, Associated Risk Factors and Current Treatment Regimes. *Curr Pharm Des*. 2019;25(38):4063-4084.

24. Vaiyapuri S, Sage T, Rana RH, et al. EphB2 regulates contact-dependent and contact-independent signaling to control platelet function. *Blood*. 2015;125(4):720-730.
25. Prevost N, Woulfe D, Tognolini M, Brass LF. Contact-dependent signaling during the late events of platelet activation. *J Thromb Haemost*. 2003;1(7):1613-1627.
26. Vaiyapuri S, Jones CI, Sasikumar P, et al. Gap junctions and connexin hemichannels underpin hemostasis and thrombosis. *Circulation*. 2012;125(20):2479-2491.
27. Vaiyapuri S, Moraes LA, Sage T, et al. Connexin40 regulates platelet function. *Nature communications*. 2013;4:2564.
28. Sohl G, Joussen A, Kociok N, Willecke K. Expression of connexin genes in the human retina. *BMC Ophthalmol*. 2010;10:27.
29. Morel S. Multiple roles of connexins in atherosclerosis- and restenosis-induced vascular remodelling. *J Vasc Res*. 2014;51(2):149-161.
30. Vaiyapuri S, Roweth H, Ali MS, et al. Pharmacological actions of nobiletin in the modulation of platelet function. *Br J Pharmacol*. 2015;172(16):4133-4145.
31. Flora GD, Sahli KA, Sasikumar P, et al. Non-genomic effects of the Pregnane X Receptor negatively regulate platelet functions, thrombosis and haemostasis. *Sci Rep*. 2019;9(1):17210.
32. Unsworth AJ, Flora GD, Sasikumar P, et al. RXR Ligands Negatively Regulate Thrombosis and Hemostasis. *Arterioscler Thromb Vasc Biol*. 2017;37(5):812-822.
33. Sáez JC, Retamal MA, Basilio D, Bukauskas FF, Bennett MV. Connexin-based gap junction hemichannels: gating mechanisms. *Biochimica et Biophysica Acta (BBA)-Biomembranes*. 2005;1711(2):215-224.
34. Malkusch S, Endesfelder U, Mondry J, Gelleri M, Verveer PJ, Heilemann M. Coordinate-based colocalization analysis of single-molecule localization microscopy data. *Histochem Cell Biol*. 2012;137(1):1-10.
35. McGuffin LJ, Atkins JD, Salehe BR, Shuid AN, Roche DB. IntFOLD: an integrated server for modelling protein structures and functions from amino acid sequences. *Nucleic Acids Res*. 2015;43(W1):W169-173.
36. Maghrabi AHA, McGuffin LJ. ModFOLD6: an accurate web server for the global and local quality estimation of 3D protein models. *Nucleic Acids Res*. 2017;45(W1):W416-w421.
37. Verselis VK, Srinivas M. Connexin channel modulators and their mechanisms of action. *Neuropharmacology*. 2013;75:517-524.
38. Leybaert L, Braet K, Vandamme W, Cabooter L, Martin PE, Evans WH. Connexin channels, connexin mimetic peptides and ATP release. *Cell Commun Adhes*. 2003;10(4-6):251-257.
39. Warner TD, Nylander S, Whatling C. Anti-platelet therapy: cyclo-oxygenase inhibition and the use of aspirin with particular regard to dual anti-platelet therapy. *British journal of clinical pharmacology*. 2011;72(4):619-633.
40. Durrant TN, van den Bosch MT, Hers I. Integrin αIIbβ3 outside-in signaling. *Blood*. 2017;130(14):1607-1619.
41. Li Z, Delaney MK, O'brien KA, Du X. Signaling during platelet adhesion and activation. *Arteriosclerosis, thrombosis, and vascular biology*. 2010;30(12):2341-2349.
42. Procter NE, Hurst NL, Nooney VB, et al. New Developments in Platelet Cyclic Nucleotide Signalling: Therapeutic Implications. *Cardiovascular drugs and therapy*. 2016;30(5):505-513.
43. Smolenski A. Novel roles of cAMP/cGMP-dependent signaling in platelets. *Journal of Thrombosis and Haemostasis*. 2012;10(2):167-176.
44. Noé L, Peeters K, Izzi B, Van Geet C, Freson K. Regulators of platelet cAMP levels: clinical and therapeutic implications. *Current medicinal chemistry*. 2010;17(26):2897-2905.
45. Walter U, Gambaryan S. cGMP and cGMP-dependent protein kinase in platelets and blood cells. cGMP: Generators, Effectors and Therapeutic Implications: Springer; 2009:533-548.
46. Gambaryan S, Kobsar A, Rukoyatkina N, et al. Thrombin and collagen induce a feedback inhibitory signaling pathway in platelets involving dissociation of the catalytic subunit of PKA from an NF-κB-IκB complex. *Journal of Biological Chemistry*. 2010:jbc. M109. 077602.
47. Unsworth A, Kriek N, Bye A, et al. PPAR γ agonists negatively regulate α II bβ3 integrin outside-in signaling and platelet function through up-regulation of protein kinase A activity. *Journal of Thrombosis and Haemostasis*. 2017;15(2):356-369.

48. Brass LF, Zhu L, Stalker TJ. Minding the gaps to promote thrombus growth and stability. *The Journal of clinical investigation*. 2005;115(12):3385-3392.
49. Brass LF, Zhu L, Stalker TJ. Novel therapeutic targets at the platelet vascular interface. *Arteriosclerosis, thrombosis, and vascular biology*. 2008;28(3):s43-s50.
50. Falk MM, Baker SM, Gumpert AM, Segretain D, Buckheit RW, 3rd. Gap junction turnover is achieved by the internalization of small endocytic double-membrane vesicles. *Mol Biol Cell*. 2009;20(14):3342-3352.
51. Falk MM, Buehler LK, Kumar NM, Gilula NB. Cell-free synthesis and assembly of connexins into functional gap junction membrane channels. *Embo j*. 1997;16(10):2703-2716.
52. Falk MM, Gilula NB. Connexin membrane protein biosynthesis is influenced by polypeptide positioning within the translocon and signal peptidase access. *J Biol Chem*. 1998;273(14):7856-7864.
53. Falk MM, Kumar NM, Gilula NB. Membrane insertion of gap junction connexins: polytopic channel forming membrane proteins. *J Cell Biol*. 1994;127(2):343-355.
54. Thomas T, Jordan K, Simek J, et al. Mechanisms of Cx43 and Cx26 transport to the plasma membrane and gap junction regeneration. *J Cell Sci*. 2005;118(Pt 19):4451-4462.
55. John SA, Revel J-P. Connexon integrity is maintained by non-covalent bonds: Intramolecular disulfide bonds link the extracellular domains in rat connexin-43. *Biochemical and Biophysical Research Communications*. 1991;178(3):1312-1318.
56. Crescente M, Pluthero FG, Li L, et al. Intracellular Trafficking, Localization, and Mobilization of Platelet-Borne Thiol Isomerases. *Arterioscler Thromb Vasc Biol*. 2016;36(6):1164-1173.
57. Taylor KA, Wright JR, Vial C, Evans RJ, Mahaut-Smith MP. Amplification of human platelet activation by surface pannexin-1 channels. *J Thromb Haemost*. 2014;12(6):987-998.
58. Molica F, Stierlin FB, Fontana P, Kwak BR. Pannexin- and Connexin-Mediated Intercellular Communication in Platelet Function. *Int J Mol Sci*. 2017;18(4).
59. Varga-Szabo D, Braun A, Nieswandt B. Calcium signaling in platelets. *J Thromb Haemost*. 2009;7(7):1057-1066.
60. Jiang L, Bardini M, Keogh A, dos Remedios CG, Burnstock G. P2X1 receptors are closely associated with connexin 43 in human ventricular myocardium. *Int J Cardiol*. 2005;98(2):291-297.
61. Unsworth AJ, Kriek N, Bye AP, et al. PPARγ agonists negatively regulate αIIbβ3 integrin outside-in signaling and platelet function through up-regulation of protein kinase A activity. *Journal of thrombosis and haemostasis : JTH*. 2017;15(2):356-369.
62. Beck F, Geiger J, Gambaryan S, et al. Time-resolved characterization of cAMP/PKA-dependent signaling reveals that platelet inhibition is a concerted process involving multiple signaling pathways. *Blood*. 2014;123(5):e1-e10.
63. Gambaryan S, Kobsar A, Rukoyatkina N, et al. Thrombin and collagen induce a feedback inhibitory signaling pathway in platelets involving dissociation of the catalytic subunit of protein kinase A from an NFkappaB-IkappaB complex. *J Biol Chem*. 2010;285(24):18352-18363.
64. Ma Y, Pitson S, Hercus T, Murphy J, Lopez A, Woodcock J. Sphingosine activates protein kinase A type II by a novel cAMP-independent mechanism. *Journal of Biological Chemistry*. 2005;280(28):26011-26017.
65. Kohr MJ, Traynham CJ, Roof SR, Davis JP, Ziolo MT. cAMP-independent activation of protein kinase A by the peroxynitrite generator SIN-1 elicits positive inotropic effects in cardiomyocytes. *J Mol Cell Cardiol*. 2010;48(4):645-648.
66. Lampe PD, Lau AF. The effects of connexin phosphorylation on gap junctional communication. *Int J Biochem Cell Biol*. 2004;36(7):1171-1186.
67. Liu J, Vitorin JFE, Weintraub ST, et al. Phosphorylation of connexin 50 by protein kinase A enhances gap junction and hemichannel function. *Journal of Biological Chemistry*. 2011:jbc. M111. 218735.
68. Ouyang X, Winbow VM, Patel LS, Burr GS, Mitchell CK, O'Brien J. Protein kinase A mediates regulation of gap junctions containing connexin35 through a complex pathway. *Molecular brain research*. 2005;135(1):1-11.

69. Pidoux G, Taskén K. Anchored PKA as a gatekeeper for gap junctions. *Communicative & Integrative Biology*. 2015;8(4):e1057361.
70. van Rijen HV, van Veen TA, Hermans MM, Jongsma HJ. Human connexin40 gap junction channels are modulated by cAMP. *Cardiovascular research*. 2000;45(4):941-951.
71. Wynn J, Shah U, Murray SA. Redistribution of connexin 43 by cAMP: a mechanism for growth control in adrenal cells. *Endocr Res*. 2002;28(4):663-668.

Figure Legends

Figure 1. Expression and localization of Cx62 in platelets (A) The presence of Cx62 was examined by immunoblot analysis of whole-cell lysates from human and mouse whole platelets, MegO1 and HeLa cells using a rabbit polyclonal anti-GJA10 antibody. Actin was used as a loading control. **(B, C)** The Localisation of Cx62 in resting and activated (with 5 μM U46619 in the presence of 3 μg/ml integrelin) permeabilized human platelets (0.2% Triton-X-100) was investigated using immunofluorescence microscopy. Cx62 (in red) and membrane GPIb receptors (in green) were stained using anti-GJA10 and anti-GPIb primary antibodies respectively. Visualization was performed using Alexa-647 and Alexa-488-conjugated secondary antibodies respectively. **(D)** The distribution of Cx62 was also studied using super-resolution STORM microscopy. Resting and activated permeabilized human platelets were stained using anti-GJA10 and anti-integrin β3 primary antibodies and visualized using Alexa-647 and Alexa-555-conjugated secondary antibodies respectively. **(E)** Coordinate-based colocalization (CBC) analysis was performed to determine the levels of Cx62 and β_3 integrin colocalization in resting (0, red line) platelets and following stimulation with thrombin (1 U/mL) for 5 minutes (300, blue line). A CBC value of zero represents a random distribution and a positive value indicates closer distribution than expected at random. Data are representative of ≥3 separate experiments.

Figure 2. Design of the ^{62}Gap27 mimetic peptide and its role in the regulation of intercellular communication. (A) Predicted 3D model of the Cx62 tertiary structure. The ribbon view of the structure is colored using the temperature coloring scheme, where blue indicates ordered regions with low predicted per-residue errors and red indicates high per-residue errors and more flexibility. **(B)** Schematic representation of the designed ^{62}Gap27 sequence on Cx62. The topological diagram of the Cx62 protomer, the predicted binding site (BS) is highlighted in orange. (NT: NH2-terminus, CL: Cytoplasmic loop, CT: COOH-terminus, T: Transmembrane, E: Extracellular) **(C)** Surface representation of Cx62 hemichannels being targeted by ^{62}Gap27 showing the pore cross-section and side views respectively. **(D)** Inter-protomer interactions. The hemichannel formed by six protomers of Cx62 is shown in grey ribbon view, the side-chains in the zoomed views are shown as sticks with brown and yellow colors to differentiate between the residues of interacting protomer pairs. **(E)** Modeled intercellular interactions between docked hemichannels. In the left-hand panel, a Cx62 gap junction channel is shown. The region enclosed by dashed lines is sectioned perpendicular to the pore axis and is viewed from the pore axis (right-hand panel). The interactions between the 2 docked hemichannels (the first external loop (E1) and the second external loop (E2) regions) are depicted in the close-up images. In region E1, Gln58 forms symmetrical hydrogen bonds with the same residue from the opposite protomer while Asn55 forms a hydrogen bond with Arg57 in the opposite protomer. In region E2, Asn196 and Asp199 form hydrogen bonds with the same residues on the opposite protomer. **(F)** The efflux of

calcein from human platelets was measured using flow cytometric analysis. Calcein loaded platelets incubated with ^{62}Gap27 or scrambled peptide (100 μg/ml) were stimulated with thrombin (0.1 U/ml). Representative histograms of calcein fluorescence for unstimulated (green), and thrombin-stimulated platelets in the presence of scrambled (blue) or ^{62}Gap27 (100μg/ml) (orange) (n=4). **(G)** Calcein efflux following thrombin stimulation for varying time periods was measured by the rate of fluorescence reduction in platelets. Median fluorescence intensity for unstimulated and stimulated samples treated with scrambled or ^{62}Gap27 was analyzed (n=4). **(H)** Calcein loaded platelets were treated with scrambled or ^{62}Gap27 (100μg/ml) for 5 minutes before their stimulation on fibrinogen and collagen-coated coverslips and FRAP analysis was performed. Representative images represent fluorescence recovery (Pre-bleach, At-bleach and Post-bleach) in samples treated with scrambled or ^{62}Gap27. Data represent Mean ± SEM, ****P<0.0001 was calculated by two-way ANOVA. **(I)** Quantified data shows mean fluorescence recovery intensity of scrambled and ^{62}Gap27 treated samples and normalized to the level of fluorescence at bleach point (shown in red circles; panel G) (n=5).

Figure 3. ^{62}Gap27 inhibits platelet activation and function specifically through Cx62. Washed human platelets (4×10^8 cells/mL) were treated with ^{62}Gap27 or scrambled peptide (S; 100 μg/ml) for 5 minutes prior to their stimulation with **(A)** CRP-XL (EC_{50}: 0.2 - 0.4 μg/ml) or **(B)** Thrombin (EC_{50}: 0.05 - 0.08 U/ml). Aggregation was measured using optical light transmission aggregometry for 180 seconds. Representative aggregation traces and quantified data shown (Scrambled-treated samples represent 100% aggregation). **(C)** Effects of ^{62}Gap27 on CRP-XL (0.25 μg/ml) and thrombin (0.05 U/ml) mediated fibrinogen binding in comparison to the scrambled peptide (S; 100 μg/ml) was evaluated in platelets (in PRP) using flow cytometry. **(D)** PRP from Cx57$^{+/+}$ and Cx57$^{-/-}$ mice was treated with ^{62}Gap27, ^{37,43}Gap27, ^{40}Gap27 (100 μg/ml) or scrambled peptide (S; 100 μg/ml) for 5 minutes. Fibrinogen binding levels were evaluated after stimulation with CRP-XL (1 μg/ml). **(E)** PRP from Cx57$^{+/+}$ and Cx57$^{-/-}$ mice was stimulated with CRP-XL (1 μg/ml) and fibrinogen binding was measured. **(F)** P-selectin exposure was measured in ^{62}Gap27 or scrambled peptide (S; 100 μg/ml) treated human platelets (in PRP), following stimulation with CRP-XL (0.25 μg/ml) or thrombin (0.05 U/ml). **(G)** Changes in ATP release were monitored for 5 minutes in washed platelets (4 x 10^8 cells/ml) incubated with ^{62}Gap27 or scrambled peptide (S; 100 μg/ml) and stimulated with CRP-XL (0.5 μg/ml) or thrombin (0.05 U/ml). **(H)** The levels of TxB_2 were measured by immunoassay in human washed human platelets (4×10^8 cells/mL) treated with scrambled peptide (S; 100 μg/ml) or ^{62}Gap27 following stimulation with CRP-XL (0.5 μg/ml) or thrombin (0.05 U/mL). Data represent mean ± SEM (n≥3), *P<0.05, **P<0.01 and ***P<0.001 was calculated by one-way ANOVA. †P<0.05 was calculated by the Student t-test.

Figure 4. ^{62}Gap27 inhibits integrin αIIbβ3-mediated signaling, thrombosis and hemostasis. (A) Human washed platelets (2×10^7 cells/mL) incubated for 5 minutes with ^{62}Gap27 (50 and 100 μg/ml) or scrambled peptide (S; 100 μg/ml) were exposed to fibrinogen (100 μg/mL) coated coverslips. Representative images of spreading and adhesion of platelets after 45 minutes and cumulative data of platelets adhered to fibrinogen in each sample are shown. Spreading platelets were categorized into 3 groups (adhered but not spread; filopodia: platelets in the process of extending filopodia; and lamellipodia: fully spread). **(B)** To measure clot retraction, human PRP was incubated with ^{62}Gap27 (50 and 100 μg/ml) or scrambled peptide (S; 100 μg/ml) for 5 minutes prior to the initiation of clot formation by the addition of thrombin (1 U/ml). The extent of clot retraction was determined by comparing clot weight after 60 minutes. **(C)** DiOC6-loaded human whole blood was treated with scrambled peptide or ^{62}Gap27 (100 μg/ml) for 5 min before perfusion through collagen-coated (100 μg/mL) Vena8Biochips at an arterial shear rate of 500 s^{-1} (20 dyne/cm^2). Representative images display thrombus formation at the end of the assay (10 mins) and quantified data represent mean thrombus fluorescence intensity. **(D)** *In vivo* thrombosis was assayed by intravital microscopy following the laser-induced injury. ^{62}Gap27 or scrambled peptide (100 μg/ml) was administered intravenously to mice, and platelets were fluorescently labeled with Alexa-647–conjugated anti-GPIb antibody. After laser injury, platelet accumulation and thrombus formation were assessed. Representative images at different time-points are shown and data are expressed as median fluorescence intensity. **(E)** The mean of maximum fluorescence intensity was calculated from the maximum fluorescence intensity of each thrombi. A total of 21 thrombi were analyzed from 5 mice treated for each condition. **(F)** Tail bleeding as determined by time to cessation of bleeding in mice treated with scrambled peptide (S) or ^{62}Gap27 (100 μg/ml) for 5 min (n=9 for scrambled peptide-treated and n=10 for ^{62}Gap27–treated samples). **(G)** The amount of blood loss was evaluated after the cessation of tail bleeding in mice treated with scrambled peptide or ^{62}Gap27 (100 μg/ml) for 5 min. Data represent mean ± SEM (n≥3), *P<0.05, **P<0.01, ***P<0.001 and ****P<0.0001 was calculated by one-way ANOVA (spreading assay), two-way ANOVA (*in vitro* thrombus formation assay), nonparametric Mann–Whitney U test (*in vivo* thrombosis and blood loss in tail-bleeding assay) and Fisher's Exact test (time to cessation of bleeding in tail bleeding assay).

Figure 5. ^{62}Gap27 inhibits GPVI signaling in human platelets. ^{62}Gap27 (50 and 100 μg/ml) or scrambled peptide (S, 100 μg/ml) pre-treated human washed platelets (4×10^8 cells/mL) were stimulated for 90 seconds with CRP-XL (1 μg/ml) under non-aggregation conditions in the presence of indomethacin (20 μM), cangrelor (1 μM), MRS2179 (100 μM) and EGTA (1 mM). Samples were lysed in the Laemmli sample buffer, separated by SDS PAGE and transferred to PVDF membranes and were tested for **A)** total tyrosine phosphorylation **(B)** Syk phosphorylation ($Tyr^{525/526}$), **(C)** LAT phosphorylation (Tyr^{200}) **(D)** PLCγ phosphorylation (Tyr^{1217}) and **(E)** PKC substrate phosphorylation. Representative blots for the phosphorylation levels are shown. The bar graph represents

mean normalized phosphorylation values relative to actin or 14-3-3-ζ levels. **(F)** FURA-2 AM–loaded washed platelets (4×10^8 cells/mL) were treated with ^{62}Gap27 or scrambled peptide (S; 100 μg/ml) for 5 minutes prior to stimulation with CRP-XL (0.25 μg/mL). Spectrofluorimetry was used to measure the release of calcium from intracellular stores. Representative traces of calcium mobilization over a period of 5 minutes and quantified data (peak calcium levels) are shown. Results are mean ± SEM (n≥3), *P<0.05 and **P<0.01was calculated by one-way ANOVA.

Figure 6. Deletion of Cx57 reduced GPVI signaling in platelets. ^{62}Gap27 (50 and 100 μg/ml) or scrambled peptide (S, 100 μg/ml) pre-treated Cx57 +/+ (WT) and Cx57 -/- (KO) washed platelets (4×10^8 cells/mL) were stimulated for 90 seconds with CRP-XL (1 μg/ml) under non-aggregation conditions in the presence of indomethacin (20 μM), cangrelor (1 μM), MRS2179 (100 μM) and EGTA (1 mM). Samples were lysed in the Laemmli sample buffer, separated by SDS PAGE and transferred to PVDF membranes and were tested for **A)** total tyrosine phosphorylation and **B)** Syk phosphorylation (Tyr$^{525/526}$), **C)** LAT phosphorylation (Tyr^{200}) and **D)** PLCγ phosphorylation (Tyr$^{1217)}$ and **E)** PKC substrate phosphorylation. Representative blots for the phosphorylation levels are shown. The bar graph represents mean normalized phosphorylation values relative to actin or 14-3-3-ζ levels. Results are mean ± SEM (n≥3), *P<0.05 and ***P<0.001 was calculated by one-way ANOVA.

Figure 7. ^{62}Gap27 modulates PKA activity independently of cAMP. (A) Resting and **(B)** CRP-XL stimulated (90 seconds) washed human platelets (4×10^8 cells/mL) treated with scrambled peptide (S; 100 μg/mL) or ^{62}Gap27 (50 and 100 μg/mL) for 5 minutes were tested for VASP S157 phosphorylation (a marker of PKA activity). VASP S157 phosphorylation was also evaluated in washed platelets treated with ^{62}Gap27 (100 μg/mL) for 5 minutes in the presence of **(C)** H89 (10 μM), **(D)** PKI (10 μM) **(F)** Rp-8-CPT-cAMPS (200 μM), **(G)** SQ 22536 (100 μM). Platelets treated with PGI_2 (1 μg/mL) for the stimulation of PKA-mediated phosphorylation were used as positive controls. The lysis of the samples was carried out using the Laemmli sample buffer prior to separation by SDS-PAGE, then the samples were transferred to PVDF membranes. 14-3-3-ζ was detected a loading control. **(E)** Levels of cAMP were measured in resting and CRP-XL (1 μg/ml) stimulated washed human platelets (4×10^8 cells/mL) that had been pre-incubated with the scrambled peptide (S; 100 μg/mL) or ^{62}Gap27 (50 or 100 μg/mL) for 5 minutes. PGI_2 (1 μg/ml) treated platelets were used as a positive control. **(H, I)** Resting washed platelets (4×10^8 cells/mL) from Cx57$^{+/+}$ and Cx57$^{-/-}$ mice were treated with scrambled peptide (S) or ^{62}Gap27 (100 μg/mL) for 5 minutes in the presence of H89 (10 μM) or Rp-8-CPT-cAMPS (200 μM) and investigated for VASP-S157 phosphorylation. Platelets treated with PGI_2 (1 μg/mL) were used as a positive control. Results are mean ± SEM (n≥4). **P<0.01 and ***P<0.001 was calculated by one-way ANOVA.

Figure 1

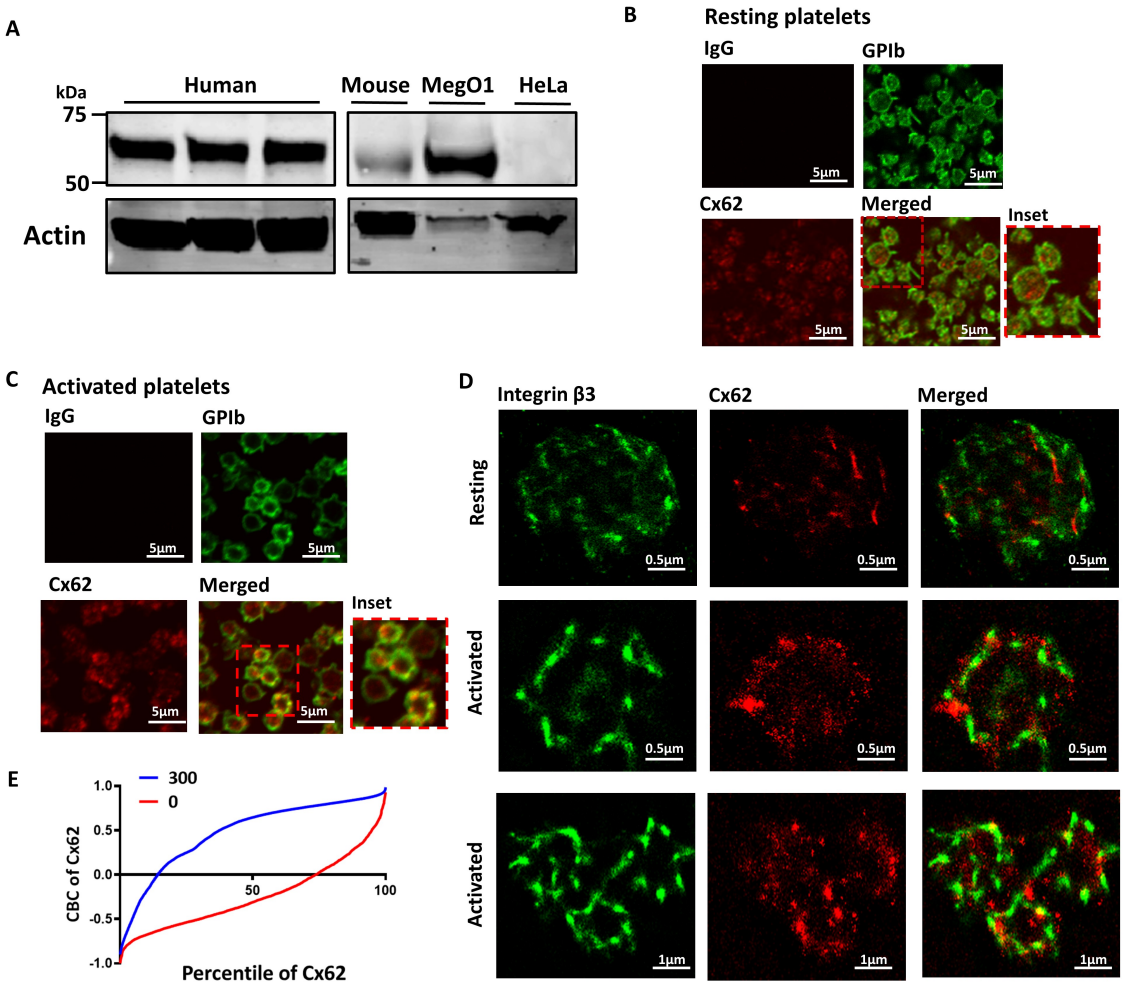
A
kDa
75
50
Actin
Human
Mouse
MegO1
HeLa
B
Resting platelets
IgG
GPIb
Cx62
Merged
Inset
5μm
C
Activated platelets
IgG
GPIb
Cx62
Merged
Inset
5μm
D
Integrin β3
Cx62
Merged
Resting
Activated
Activated
0.5μm
1μm
E
300
0
CBC of Cx62
1.0
0.5
0.0
-0.5
-1.0
50
100
Percentile of Cx62

Figure 2

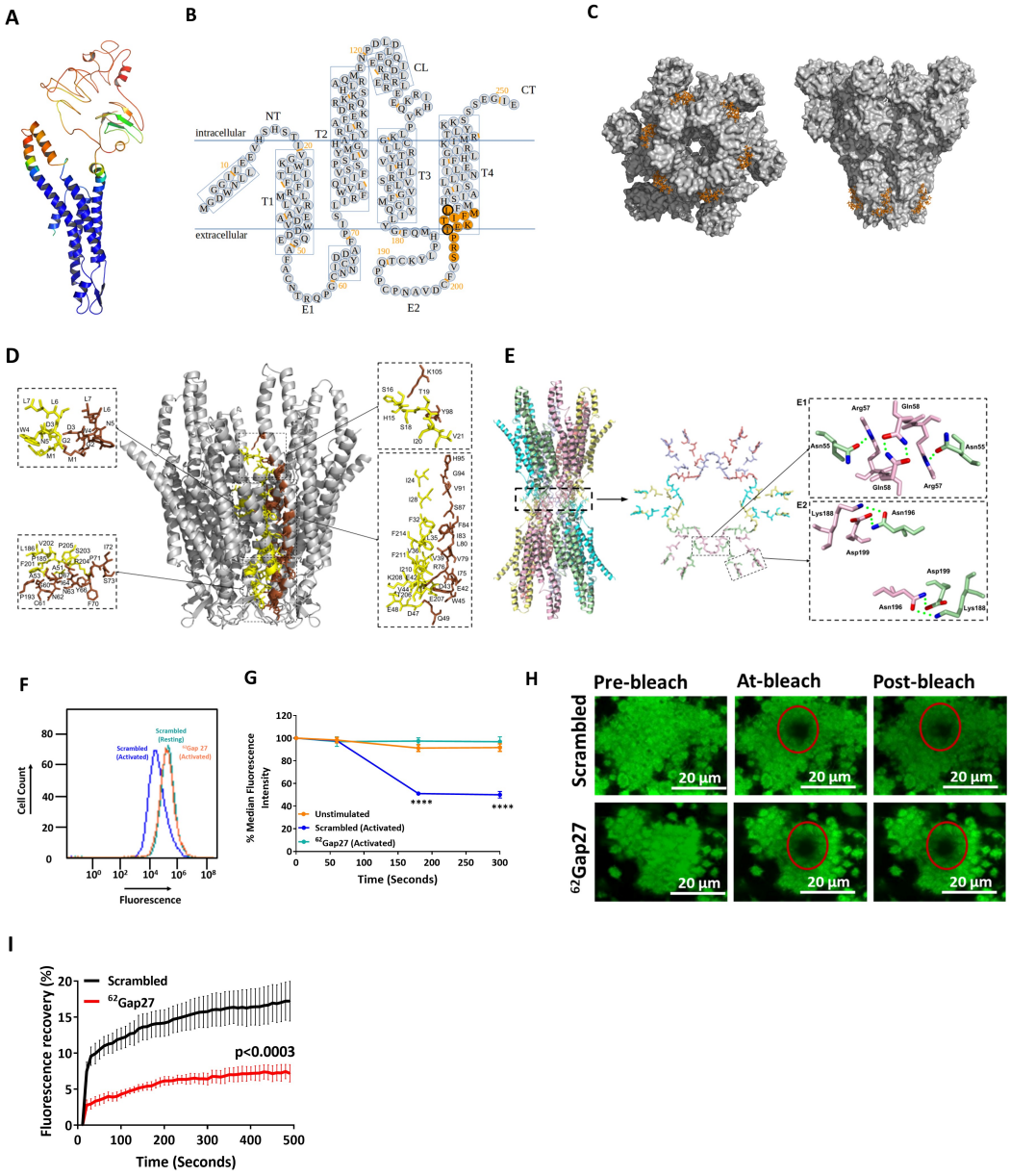
A
B
C
D
E
F
G
H
I
NT
CT
CL
T1
T2
T3
T4
E1
E2
intracellular
extracellular
Cell Count
Fluorescence
Scrambled (Resting)
Scrambled (Activated)
62Gap 27 (Activated)
% Median Fluorescence Intensity
Time (Seconds)
Unstimulated
Scrambled (Activated)
62Gap27 (Activated)
Pre-bleach
At-bleach
Post-bleach
Scrambled
62Gap27
20 µm
Fluorescence recovery (%)
Scrambled
62Gap27
p<0.0003
Time (Seconds)

Figure 3

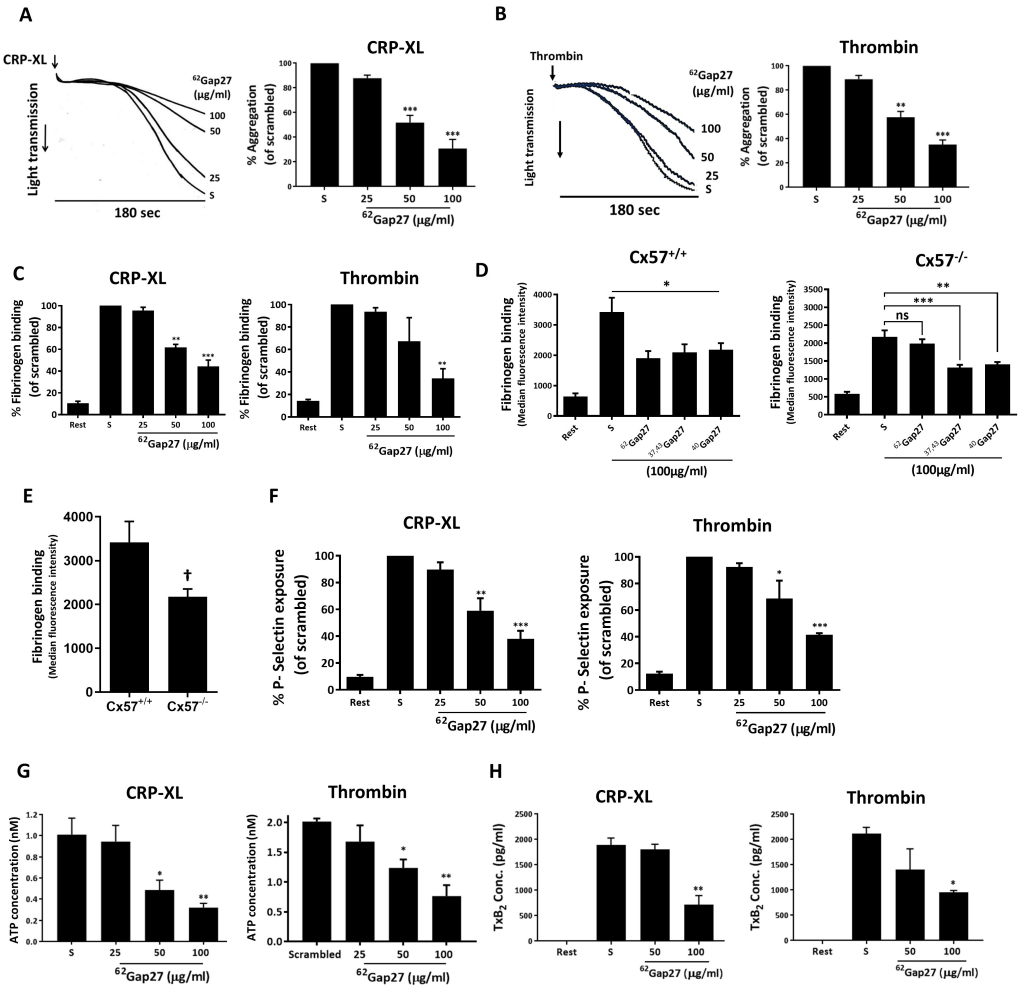
A
CRP-XL
Light transmission
180 sec
62Gap27 (µg/ml)
100
50
25
S
% Aggregation (of scrambled)
62Gap27 (µg/ml)
B
Thrombin
C
CRP-XL
Thrombin
% Fibrinogen binding (of scrambled)
Rest
D
Cx57+/+
Cx57-/-
Fibrinogen binding (Median fluorescence intensity)
(100µg/ml)
ns
E
Cx57+/+
Cx57-/-
F
% P- Selectin exposure (of scrambled)
G
ATP concentration (nM)
Scrambled
H
TxB2 Conc. (pg/ml)

Figure 4

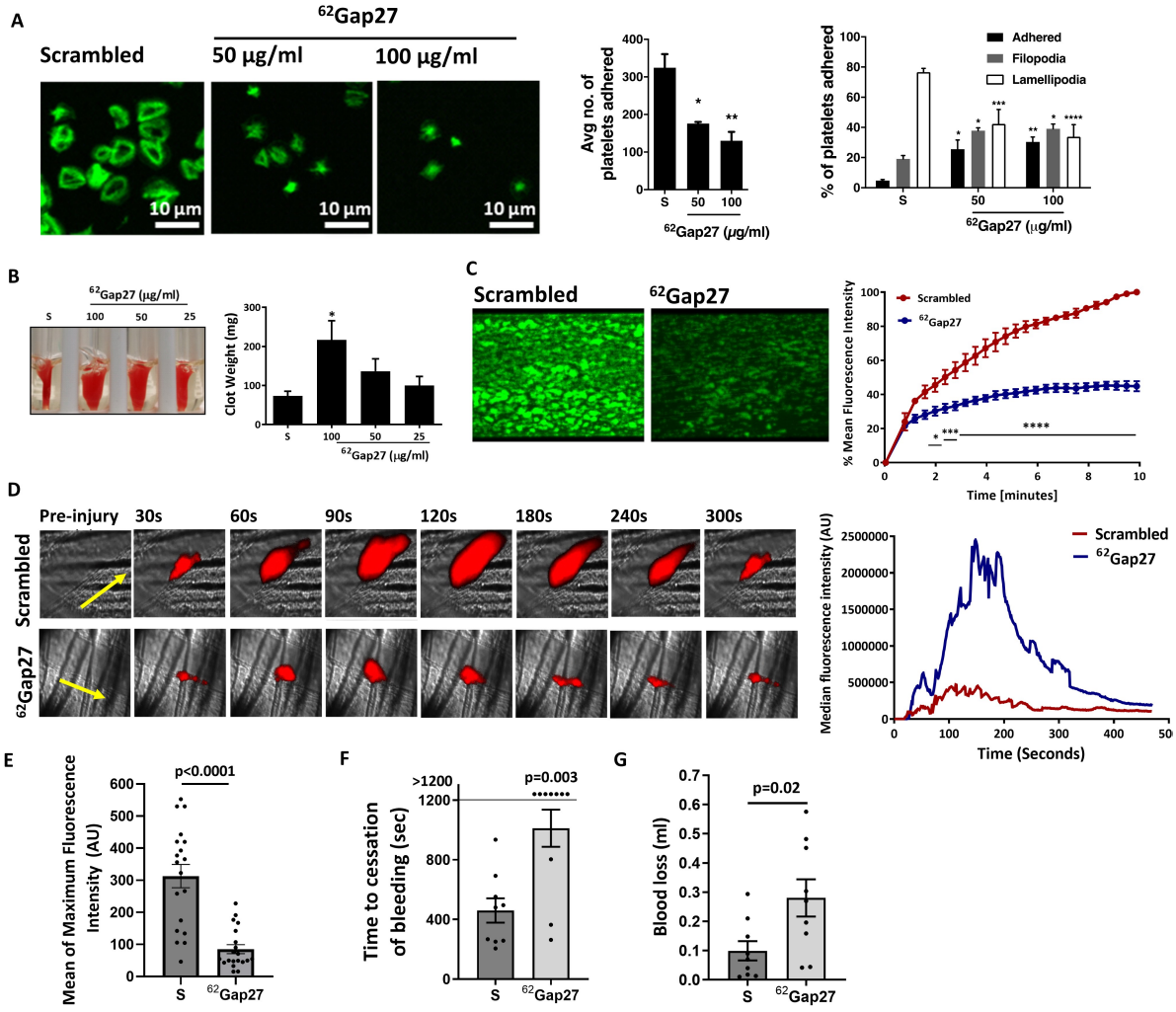
A
Scrambled
62Gap27
50 µg/ml
100 µg/ml
10 µm
Avg no. of platelets adhered
62Gap27 (µg/ml)
% of platelets adhered
Adhered
Filopodia
Lamellipodia
B
62Gap27 (µg/ml)
Clot Weight (mg)
C
Scrambled
62Gap27
% Mean Fluorescence Intensity
Time [minutes]
D
Pre-injury
30s
60s
90s
120s
180s
240s
300s
Median fluorescence intensity (AU)
Time (Seconds)
E
Mean of Maximum Fluorescence Intensity (AU)
p<0.0001
F
Time to cessation of bleeding (sec)
p=0.003
G
Blood loss (ml)
p=0.02

Figure 5

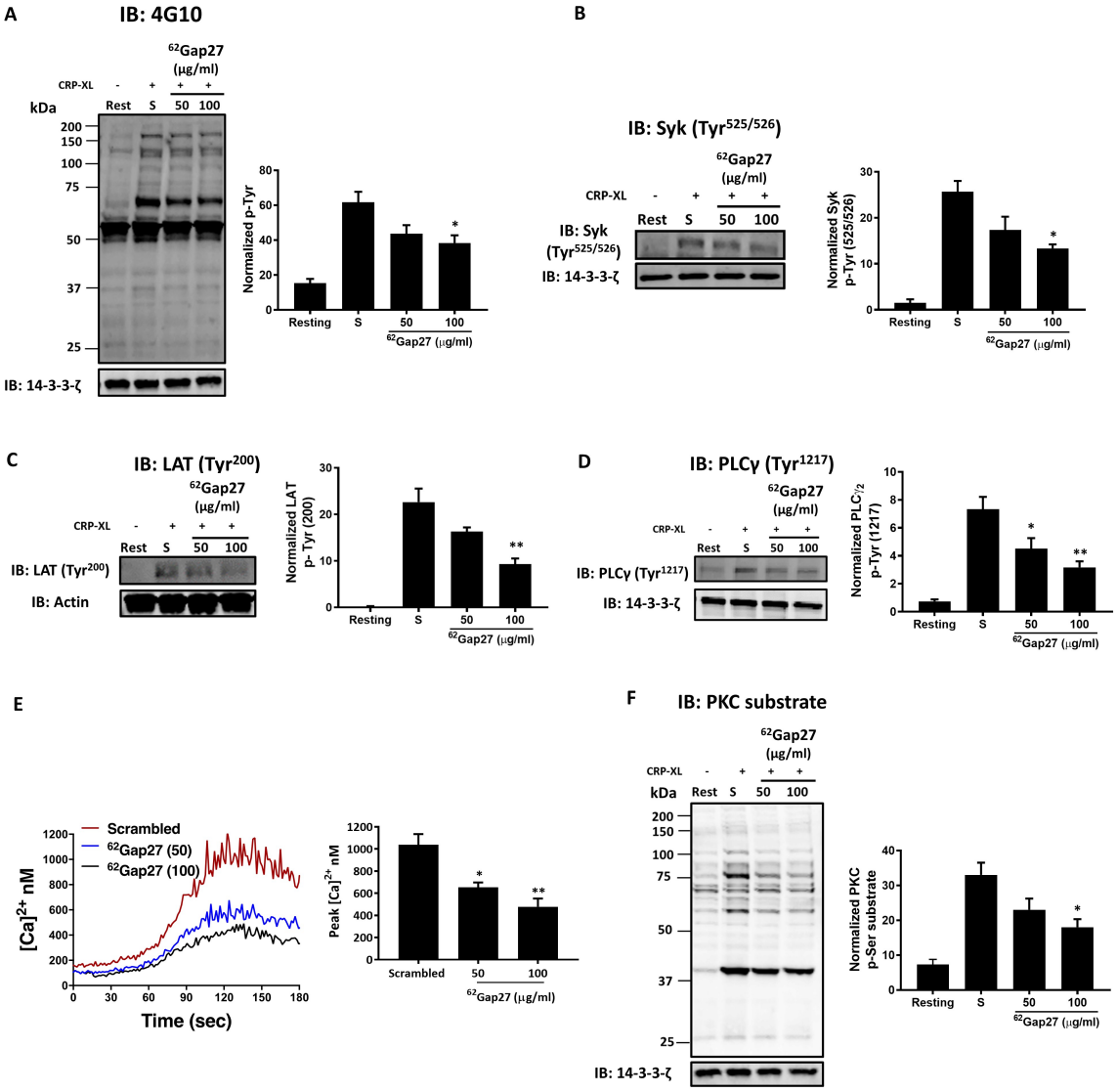
A
IB: 4G10
62Gap27 (μg/ml)
CRP-XL
kDa
Rest
S
50
100
200
150
100
75
50
37
25
IB: 14-3-3-ζ
Normalized p-Tyr
Resting
62Gap27 (μg/ml)
B
IB: Syk (Tyr525/526)
IB: Syk (Tyr525/526)
IB: 14-3-3-ζ
Normalized Syk p-Tyr (525/526)
C
IB: LAT (Tyr200)
IB: LAT (Tyr200)
IB: Actin
Normalized LAT p- Tyr (200)
D
IB: PLCγ (Tyr1217)
IB: PLCγ (Tyr1217)
IB: 14-3-3-ζ
Normalized PLCγ2 p-Tyr (1217)
E
Scrambled
62Gap27 (50)
62Gap27 (100)
[Ca]2+ nM
Time (sec)
Peak [Ca]2+ nM
Scrambled
F
IB: PKC substrate
IB: 14-3-3-ζ
Normalized PKC p-Ser substrate

Figure 6

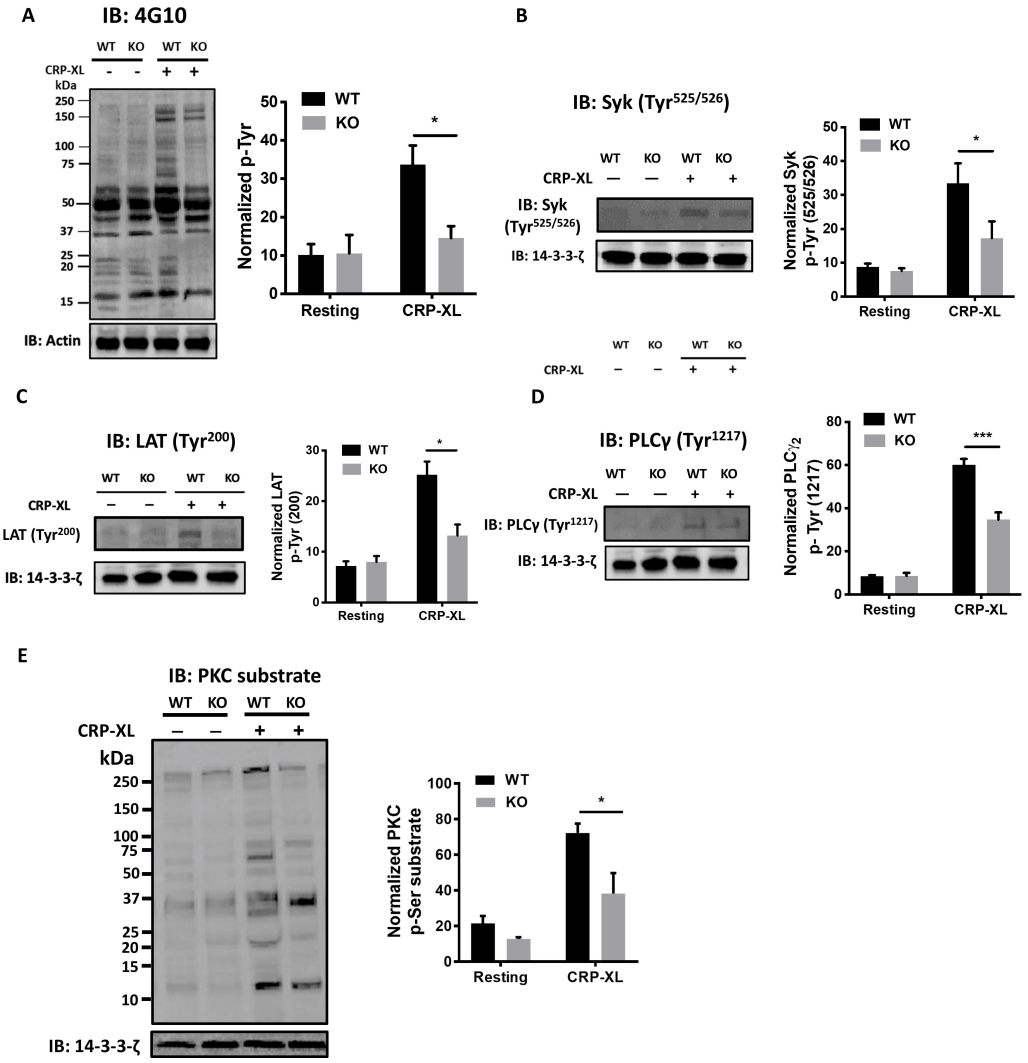
A
IB: 4G10
WT KO WT KO
CRP-XL - - + +
kDa
250
150
100
75
50
37
25
20
15
IB: Actin
WT
KO
Normalized p-Tyr
Resting
CRP-XL
B
IB: Syk (Tyr525/526)
IB: Syk (Tyr525/526)
IB: 14-3-3-ζ
Normalized Syk p-Tyr (525/526)
C
IB: LAT (Tyr200)
IB: LAT (Tyr200)
IB: 14-3-3-ζ
Normalized LAT p-Tyr (200)
D
IB: PLCγ (Tyr1217)
IB: PLCγ (Tyr1217)
IB: 14-3-3-ζ
Normalized PLCγ2 p- Tyr (1217)
E
IB: PKC substrate
IB: 14-3-3-ζ
Normalized PKC p-Ser substrate

Figure 7

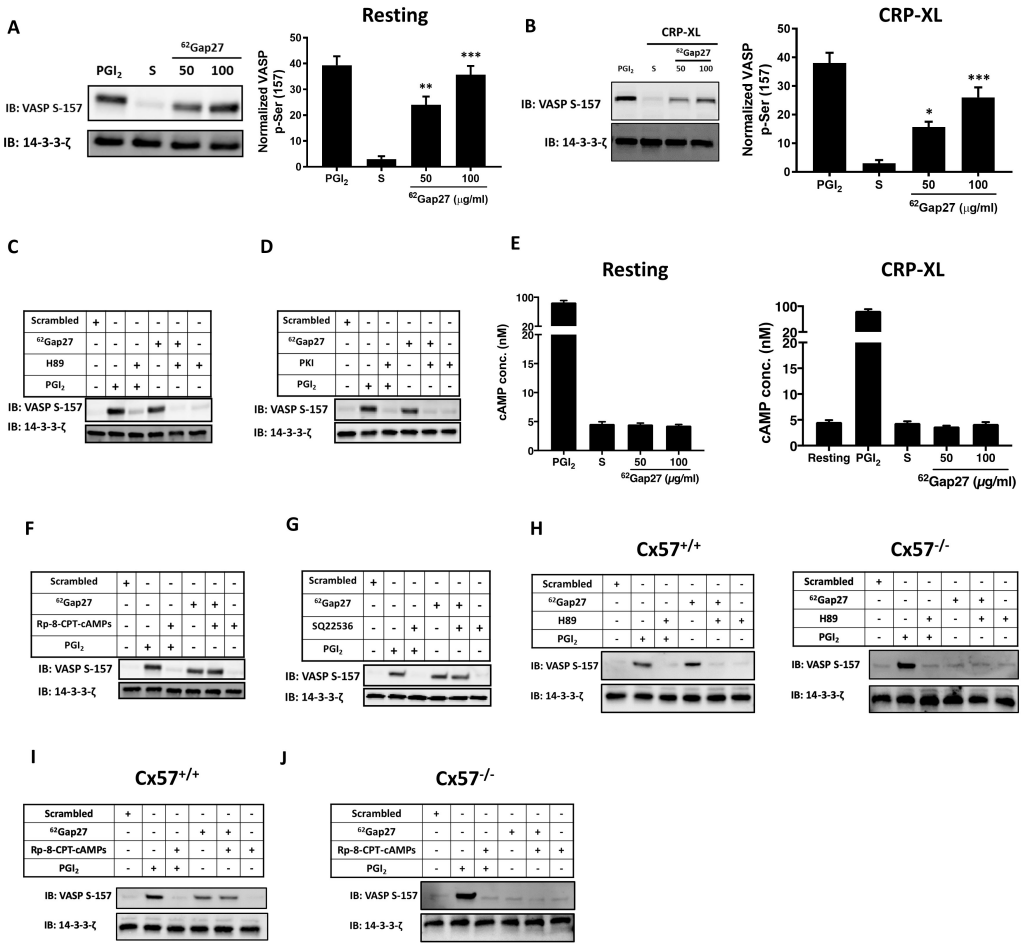
A
Resting
PGI2
S
62Gap27
50
100
IB: VASP S-157
IB: 14-3-3-ζ
Normalized VASP p-Ser (157)
62Gap27 (μg/ml)
B
CRP-XL
C
D
E
cAMP conc. (nM)
Scrambled
62Gap27
H89
PKI
F
Rp-8-CPT-cAMPs
G
SQ22536
H
Cx57+/+
Cx57-/-
I
J

Supplemental information

Structural, Functional and Mechanistic Insights Uncover the Fundamental Role of Orphan Connexin 62 in Platelets

Authors

Khaled A. Sahli,[1,2] * Gagan D. Flora,[1,3] * Parvathy Sasikumar,[1,4] Ali H. Maghrabi,[1] Lisa-Marie Holbrook,[1,5], Sarah K. AlOuda,[1] Amro Elgheznawy[1], Tanya Sage,[1] Alexander R. Stainer,[1] Recep Adiyaman,[1] Mohammad AboHassan,[1] Marilena Crescente,[1,6] Neline Kriek[1], Sakthivel Vaiyapuri[1,7], Alexander P. Bye,[1] Amanda J. Unsworth[1,8], Christopher I. Jones[1], Liam J. McGuffin,[1] Jonathan M. Gibbins[1]

KAS and GDF contributed equally to this study and are joint first authors

Materials

Cx62 antibody was obtained from Sigma-Aldrich. The anti-phosphotyrosine antibody 4G10 was obtained from Millipore, USA and the phospho-specific antibodies - PLCγ2 (Y759), AKT (S473), myosin light chain (S19) and vasodilator-stimulated phosphoprotein (VASP) phospho-Ser157 and Ser239 were obtained from cell signaling technologies, USA. Syk (pY525/526) and LAT (Y200) antibodies were from Abcam. Anti-Phospho–PKC substrate antibody was purchased from New England BioLabs, USA. Mouse anti-human 14-3-3ζ (Santa Cruz Biotechnology, USA) was used to detect 14-3-3ζ to ensure equivalent levels of protein loading in immunoblots. The secondary antibodies used for immunoblotting; Cy5 goat anti-rabbit IgG, AlexaFluor488 goat anti-rabbit and AlexaFluor 488 goat anti-mouse IgG antibodies were obtained from Life Technologies, UK. All other reagents were from previously described sources[1-3].

Methods

Preparation of human Platelets

Human blood was taken from consenting, drug-free volunteers on the day of the experiment according to the methodology approved by the University of Reading Research Ethics Committee. Blood was taken using 3.8% (w/v) sodium citrate and Acid Citrate Dextrose (ACD; 110 mmol/L glucose, 80 mmol/L citric acid, 120 mmol/L sodium citrate) as an anticoagulant. Whole blood was centrifuged at 102*g* for 20 minutes at 20°C to yield platelet-rich plasma (PRP). Where washed platelets were required, they were isolated from the PRP by further centrifugation at 1413*g* for 10 minutes at 20^{o}C in the presence of 0.1 µg/ml prostacyclin to prevent activation. The supernatant was discarded in Klorsept disinfectant (Medentech, Wexford, Ireland) and the platelet pellet was resuspended in 25ml of modified Tyrodes-HEPES buffer (134 mmol/L NaCl, 0.34 mmol/L Na_2HPO_4, 2.9 mmol/L KCl, 12 mmol/L $NaHCO_3$, 20 mmol/L HEPES, 5 mmol/L glucose, 1 mmol/L $MgCl_2$, pH 7.3) and 3 ml of ACD in the presence of 0.1 µg/ml prostacyclin. Platelets were centrifuged at 1413*g* for 10 minutes at 20^{o}C and resuspended to a density of $4x10^8$ cells/ml in modified Tyrodes-HEPES buffer using a platelet count obtained with a Z Series Coulter Counter (Beckman Coulter, CA, USA). Washed platelets were rested for at least 30 minutes at 30^{o}C prior to the experiment to allow

responses to recover. Platelet preparations typically contained fewer than 1 contaminating erythrocyte or leukocyte per 6500 platelets.

ADP-sensitive washed platelets were prepared by collecting blood into 3.8% (w/v) sodium citrate and centrifugation at 102*g* for 20 minutes at 20°C to yield PRP (without the addition of ACD). Platelets were isolated from the PRP by further centrifugation at 350*g* for 20 minutes. The supernatant was discarded, and the platelet pellet was resuspended to a density of $4x10^8$ cells/ml in the modified Tyrodes-HEPES buffer.

Preparation of Mouse Platelets

Mouse blood was collected through cardiac puncture after termination by rising CO_2 concentration and cervical dislocation as per Schedule 1 of the Animals (Scientific Procedures) Act 1986. After the mice were euthanized, their blood was drawn through the cardiac puncture into a syringe containing 4% sodium citrate (1 part sodium citrate to 9 parts blood). Red blood cells and leukocytes were eliminated by reducing the concentration of blood with Tyrode's-HEPES buffer followed by centrifugation at 203 *g* for 8 minutes. The upper layer comprising PRP was gently aspirated with a pipette. After the addition of PGI_2 (final concentration, 12.5 ng/mL) to the PRP, the platelets were subjected to centrifugation at 1,028 *g* for 5 minutes. The resulting platelet pellet was resuspended in modified Tyrode's-HEPES buffer (4×10^8 cells/mL) and left to rest at 30°C for 30 minutes.

Sucrose gradient sub-cellular fractionation

Platelet fractionation was performed as previously described with minor modifications[4]. Platelets were transferred into a cell-disruption bomb (Parr 4639, Parr Instrument Co.) and homogenized by nitrogen cavitation. A pressure of 1200 psi was applied with N_2 to the platelet suspension and after 15 min the pressure was quickly released. This procedure was repeated three times and the final platelet homogenate was cleared from the cell debris and partially disrupted cells by centrifugation at 500g for 10 min. The platelet homogenate was fractionated over a linear sucrose gradient (from 60 to 30%, w/v in 5mM EDTA) by centrifugation at 284,061 x g for 2 hours at 4°C. Fractions were collected from the top of the tube and aliquots analyzed by immunoblotting.

Immunofluorescence microscopy

Human blood was collected in vacutainers containing sodium citrate as described previously. The blood was centrifuged at 100g for 20 minutes to collect PRP. Resting or activated platelets (stimulated with 5 µM U46619; in the presence of 4 µM integrillin) in PRP were fixed with an equal volume of 8% paraformaldehyde-PBS (PFA-PBS) to make a final concentration of 4% (v/v) and incubated for 15 min. Thereafter, platelets were centrifuged at 950g for 10 minutes. The supernatant was removed, and the platelet pellet was resuspended in 2 ml of PBS-ACD (pH 6.1) for washing. Platelets were centrifuged for 10 minutes at 950g and resuspended in 1 ml of PBS-ACD to concentrate platelets. Platelets were centrifuged again at the same speed for 10 minutes and then resuspended in 500µl of 1% (w/v) BSA-PBS, to concentrate platelets even more. Poly-L-lysine coated-12mm coverslips (VWR micro cover glass No.1.5) were put in a 6x6 culture plate and 90µl of platelets were added on each coverslip. Culture plates were placed at 37^{o}C for 90 minutes. After 2-3 washes with PBS, samples were blocked with 0.2% (v/v) Triton-X-100, 2% (v/v) serum from same species as secondary antibody and 1% (w/v) protease-free BSA for 1h. Thereafter, primary antibodies diluted (1:100) in 0.2% (v/v) Triton-X-100, 2% (v/v) serum from the same species as secondary antibody and 1% (w/v) protease-free BSA were added and left overnight. The following day, samples were washed with PBS (2-3 times) and secondary antibodies (1:200) were added for 1 hour at room temperature. The unbound antibodies were washed off with PBS (2-3 times) and samples were fixed using 4% (v/v) PFA-PBS for 5 minutes. The coverslips were washed again with PBS (2-3 times). Coverslips were placed on glass slides after adding ProLong Gold Antifade mounting media (Life technologies). The slides were kept at room temperature until mounting media dried and then kept in the fridge until they were imaged using a Nikon A1-R confocal microscope (100x oil immersion).

Stochastic optical reconstruction microscopy (STORM)

Tyrode's-HEPES buffer was used to dilute the PRP (1:20). The polymerization of fibrin was prevented by treatment with GPRP (0.5 mg/mL). The samples were activated with thrombin (1 U/mL) for 5 minutes, then the unstimulated and stimulated samples were fixed with 2% (v/v) formyl saline and subjected to centrifugation for 15 minutes at 500 *g*. After removal of the supernatants, the pellets containing the platelets were resuspended in Perm Buffer III (100 µL; BD Biosciences, Oxford, UK) and incubated on ice for 30 minutes. Platelets were then washed with Tyrode's-HEPES buffer (2 × 20 minutes) and subjected to centrifugation at 500 *g*. The supernatant

was discarded, and the resultant pellet was resuspended in Tyrode's-HEPES buffer (50 µL). The samples were incubated with the primary antibodies (diluted 1:50; mouse monoclonal IgG against integrin β_3 and rabbit polyclonal IgG against Cx62) at 4 °C overnight. Platelets were then washed twice with Tyrode's-HEPES buffer (2 mL) followed by centrifugation for 20 minutes at 550 *g*. The samples were incubated with secondary antibodies (diluted 1:50 in Tyrode's-HEPES buffer; Alexa Fluor® 647-labeled donkey anti-rabbit to detect Cx62 and Alexa Fluor® 555-labeled goat anti-mouse to detect β_3 integrin) at 37 °C for 30 minutes. Platelets were then washed with Tyrode's-HEPES buffer (2 mL) and subjected to centrifugation for 20 minutes at 550 *g*. The resulting pellet was suspended in Tyrode's-HEPES buffer (100 µL). Finally, platelets (100 µL) were applied to the ibidi® slides coated with poly-L-lysine. The slides were incubated at 4 °C overnight to allow the platelets to adhere. The next day, the unbound platelets were removed and blinking buffer was added (Stock A: 0.90 g/mL catalase [Sigma–Aldrich], 0.182 mM Tris [2-carboxyelthyl] phosphine hydrochloride [Sigma–Aldrich], 2.27% [v/v] glycerine, 1.14 mM KCl, 0.91 mM Tris-HCl [pH 7.5], 0.045 mg/mL glucose oxidase [Sigma–Aldrich] and 5 mL diH_2O; stock B: 36 mg/mL glucose, 3.6% [v/v] glycerine and 36 mL H_2O; and stock C: 0.09 M mercaptoethylamine-HCl [Sigma–Aldrich] and 1 mL diH_2O). For 3D STORM imaging of the platelets, the 100× oil immersion lens of the microscope was used.

Coordinate-based colocalization (CBC) analysis[5] was performed to assess changes in the colocalization of Cx62 and β_3 integrin upon platelet stimulation using ImageJ and the open-source Thunderstorm plugin.[6]

Calcein Dye Efflux

Platelets (in PRP) were loaded with calcein-AM (0.5 µM; Thermo Fisher Scientific, Waltham, MA, USA) for 30 minutes at 37 °C as described previously [7]. The platelets were then treated with scrambled peptide or ^{62}Gap27 for 5 minutes. Next, the platelets were stimulated with thrombin (0.1 U/mL). In order to prevent fibrin polymerization, the thrombin-treated samples were also treated with GPRP (25 µg/mL). Stimulation was carried out with gentle mixing for different time periods over 5 minutes. Finally, the reaction was stopped with 0.2% (v/v) formyl saline. Flow cytometry (488 nm excitation, 530 ± 30 nm emission) was performed with a BD Accuri™ C6 flow cytometer (BD Biosciences, Oxford, UK). For each sample, 10,000 events, gated on platelets by

forward scatter and side scatter, were collected. Data were analyzed with the built-in BD Accuri™ C6 Plus software (version 1.0.264.21).

Fluorescence Recovery after Photobleaching (FRAP)

FRAP analysis was performed as previously described with minor modifications[8,9]. Each of eight wells of each ibidi® slide was coated with fibrinogen (100 μg/mL) and collagen (10 μg/mL) in modified PBS for 1 hour. 1% (w/v) BSA was added to the wells followed by a 1-hour incubation to prevent the binding of platelets to the glass. The wells were washed three times with PBS. Calcein-loaded PRP was added to the coated coverslips and incubated for 45 minutes. Unbound platelets were washed from the wells with PBS (three washes). The samples were then treated with the scrambled peptide or ^{62}Gap27 (100 μg/mL) for 5 minutes. A high-intensity laser (488 nm) was trained on the central circular area (8-μm-diameter region of interest [ROI]) of the monolayer of cells thrombus for 300 milliseconds, resulting in an 85% loss of fluorescence. Then, a 488-nm wavelength laser was used to excite the samples and the fluorescence emission was detected at 500–520 nm. Finally, fluorescence recovery was recorded for 500 seconds. The 100× oil immersion objective of an A1R confocal microscope was used to capture images of single sections every second for 500 seconds. Five thrombi from each of seven donor samples treated with scrambled peptide or ^{62}Gap27 were analyzed. NIS-Elements software (Nikon, Tokyo, Japan) was used to compute the mean fluorescence intensities. For each time point, the average fluorescence intensities were computed for the background, non-bleached (reference) and bleached areas.

Protein Bioinformatics

The complete sequence of Cx62 was obtained from GenBank[10], and for the physicochemical analysis, ProtParam[11] was utilized. In the absence of an experimental structure, state-of-art structure prediction tools were employed to obtain 3D models for the Cx62 protomer. The IntFOLD4-TS method[12] from the IntFOLD server[13] was used to predict tertiary structure models for the Cx62 protomer (monomeric subunit). Additionally, the quality estimation method, ModFOLD6[14], was employed to provide both global and local (per-residue) scores for estimating 3D model quality. The calculated local (or per-residue) errors from ModFOLD6 were mapped onto the model using the temperature coloring scheme ranging from blue (indicating residues modeled

with high quality) to red (indicating residues with lower model quality, which are often more flexible or disordered).

Multiple sequence alignment of human connexin sequences was performed using ClustalW to ensure the selectivity of 62Gap27. A scrambled peptide control was designed using Mimotopes, (http://www.mimotopes.com/peptideLibraryScreening.asp?id=97) and BLAST searches performed to ensure that designed sequences were not present in any other proteins.
To predict the most likely interactions occurring between Cx62 and the ^{62}Gap27 inhibitor, protein-ligand docking was performed using the SwissDock server[15]. The FullFitness and Gibbs free energy (ΔG) score of each run of the docking was evaluated and the final ranking of each cluster was based on the FullFitness scores.

The quaternary structures of the Cx62 hemichannels (2x 6-mers) were successfully modeled using the PDB entry 2zw3 (crystal structure of Cx26 gap junction) as a template. The docked hemichannel assembly (12-mer) template for PDB ID 2zw3 was downloaded from PISA [16] service at the EBI (http://www.ebi.ac.uk/pdbe/prot_int/pistart.html). For each hemichannel, the template was used to orientate six of the modeled protomers by a six-fold symmetry axis perpendicular to the membrane plane and build the complete model of the docked hemichannel (12-mer) complex. Residues in the modeled protein-protein and protein-ligand complexes were considered to be interacting if the distance between the closest heavy atoms (i.e. non-hydrogen) in the residues belonging to different chains was <= 5Å

Platelet aggregometry

Light transmission aggregometry (LTA) was performed in an optical platelet aggregometer (Chrono-Log, PA, USA, and Helena Biosciences Europe, Gateshead, UK). Washed platelets (4x10^8 cells/ml) treated with ^{62}Gap27 or scrambled peptide were stimulated in the presence of agonist (collagen, CRP-XL, thrombin, U46619 or ADP) with continuous stirring (1200 rpm at 37^{o}C) for 3 minutes and aggregation was measured as an increase in light transmittance. The data were quantified by considering scrambled peptide-treated samples as 100% aggregation and the level of aggregation obtained in scrambled peptide-treated samples was normalized to it.

Fibrinogen binding and alpha granule secretion

Fibrinogen binding and P-selectin exposure to the platelet surface were detected by flow cytometry as measures of integrin αIIbβ3 activation and the secretion of α-granules respectively. Fluorescein isothiocyanate (FITC)-labelled rabbit anti-human fibrinogen antibody (Dako, Ely, UK) was used to measure fibrinogen binding. PE-Cy™ 5-labeled mouse anti-human CD62P antibody (BD Biosciences, Oxford, UK) was used to measure the exposure of P-selectin. The assay volume comprising human or mouse PRP, an inhibitor of Cx function or appropriate scrambled peptide control and each of the antibodies in modified Tyrode's-HEPES buffer, was incubated for 5 minutes at room temperature in the dark. The platelet agonists thrombin (in the presence of GPRP to prevent fibrin polymerization) or CRP-XL were added and incubated for an additional 20 minutes. The reaction was stopped by the addition of 0.2% (v/v) formyl saline. A BD Accuri™ C6 flow cytometer (BD Biosciences, Oxford, UK) and BD Accuri™ C6 software were used for the acquisition of the flow cytometry data. The median fluorescence intensity was calculated for 10,000 gated events. Fluorescence in FL1-A and FL3-A channels were used to analyze fibrinogen binding and P-selectin exposure, respectively.

Dense granule secretion

Dense granule secretion was determined by measuring changes in the extracellular ATP concentration. These changes were observed concurrently with aggregation in a Model 700 Whole Blood/Optical Lumi-Aggregometer with the use of a luciferase kit (Chrono-Log, Havertown, PA, USA). ATP release from dense granules was monitored with a bioluminescence system comprising D-luciferin, firefly luciferase and magnesium. ATP interactions with these reagents produce light, in direct proportion to the ATP concentration, which is observed and quantified using a Lumi-aggregometer. Platelets (4×10^8 cells/mL) were pre-treated with ^{62}Gap27 or scrambled peptide at 37°C for 5 minutes. Luciferase was added under stirring conditions during the last 2 minutes of the incubation. The platelets were stimulated with the indicated concentrations of thrombin or CRP-XL under stirring conditions (1,200 rpm at 37°C). ATP release and aggregation at 37°C were recorded for 3 minutes following the addition of agonist using the AggroLink8 software, which calculates ATP secretion levels from the 2nM ATP standard.

TxB_2 Assay

The TxB_2 measurements were performed with a TxB_2 immunoassay kit based on a competitive ELISA (Cayman Chemical, Cambridge, UK), according to the manufacturer's instructions. Washed platelets (4×10^8 cell/mL) were treated with ^{62}Gap27 or scrambled peptide for 5 minutes in glass cuvettes. The samples were then activated with CRP-XL or thrombin. After 5 minutes, stop solution (1 mM EGTA and 10 µM indomethacin) was added to terminate the reaction. The samples were then immediately subjected to centrifugation for 2 minutes at 12,000 rpm and the supernatants were frozen at −80°C. Later, the supernatants were thawed and diluted 1:40 in ELISA buffer (0.01% [w/v] sodium azide, 1 mM EDTA, 400 mM NaCl, 0.1% [w/v] BSA and 100 mM phosphate). The dilutions were plated in wells coated with polyclonal goat anti-mouse IgG antibodies. To determine the relationship between the TxB_2 concentration and absorbance, TxB_2 standards were prepared. TxB_2-acetylcholinesterase and anti-TxB_2 monoclonal antibody were added to each well, then the plate was incubated at room temperature for 2 hours. After incubation, the plate was washed 4 times with washing buffer. Next, Ellman's reagent was added to each well and the plate was incubated in the dark. A NOVOstar plate reader (BMG Labtech, Aylesbury, UK) was used to determine the absorbances of the wells at 405 nm. A standard curve was plotted using the absorbance readings for the TxB_2 standards. The inverse function was used to compute the TxB_2 concentrations from the test sample readings.

Measurement of intracellular calcium mobilization

The mobilization of Ca^{2+} from intracellular stores into the platelet cytosol was measured in a fluorescence-based 96-well plate assay. PRP was incubated with 2 µM Fura-2 AM for 60 minutes at 30°C. The PRP was washed and subjected to centrifugation at 350 *g* for 20 minutes, then resuspended in modified Tyrode's-HEPES buffer containing $CaCl_2$ $(1mM)$ at 4×10^8 cell/mL. Fura-2-loaded platelets were incubated with ^{62}Gap27 or scrambled peptide for 5 minutes at 37°C, then stimulated with the agonists, CRP-XL or thrombin. A NOVOstar plate reader (BMG Labtech, Aylesbury, UK) was used to measure the fluorescence (excitation at 340 and 380 nm and emission at 510 nm). The ratio of the excitation signals at 340 and 380 nm was used to estimate the concentration of Ca^{2+}. To measure the mobilisation of calcium from intracellular stores, the

above-mentioned steps were performed using Fura-2 loaded washed platelets (in the absence of 1 mM $CaCl_2$) in the presence of saturating concentration of EGTA (2mM).

The cells were lysed with digitonin (5 µM) to release the Fura-2 into the assay buffer (which contained 1 mM $CaCl_2$) and facilitate the measurement of the maximum fluorescence ratio. The minimum fluorescence ratio was measured by chelating Ca^{2+} ions with EGTA (10 mM) and Tris base (10 mM; added to ensure that the pH remained alkaline for optimum Ca^{2+} buffering by EGTA). Non-Fura-2-loaded cells at the same final density were used to measure the autofluorescence levels. Using the calibration values from above, experimental $[Ca^{2+}]_i$ concentrations were calculated using the following equation:

$$[Ca^{2+}]_i = K_d \times \frac{S_f}{S_b} \times \frac{R - R_{min}}{R_{max} - R}$$

Where K_d is the dissociation constant of Fura-2AM (~224 nM). S_f and S_b are the values of the fluorescence at 380nm excitation (corrected to background auto-fluorescence), with zero or saturating $[Ca]^{2+}$ respectively. R is the 340/380nm fluorescence ratio, corrected for background fluorescence. R_{min} and R_{max} are the ratio limits at zero or saturating $[Ca]^{2+}$, respectively, adjusted using a viscosity constant of 0.85. This corrects for the effects of the cellular environment on the fluorescence of Fura-2.

Platelet adhesion and spreading

To study platelet spreading, glass coverslips coated with fibrinogen (100 µg/mL in modified PBS) were placed in 6-well plates. After coating for 1 hour, 1% (w/v) BSA was added to the coverslips followed by 60 minutes incubation to prevent platelets from binding the glass. The coverslips were then washed three times with PBS. The washed platelet suspensions (2×10^7 cells/mL) that had been incubated for 5 minutes with ^{62}Gap27 or scrambled peptide were then added to the coverslips and incubated at 37°C for 45 minutes. Unbound platelets were removed, and the coverslips were washed three times with PBS. Then, the coverslips were fixed in 0.2% (v/v) formyl saline for 10 minutes. The coverslips were again washed three times with PBS. Next, the platelets were permeabilized with 0.2% (v/v) Triton™ X-100 for 5 minutes, then washed three times with PBS. The coverslips were incubated with Alexa Fluor® 488-conjugated phalloidin for 1 hour in the dark to label filamentous actin. The supernatants were removed, the coverslips were washed with PBS and placed on glass slides and fluorescence was preserved by adding ProLong™ Gold Antifade

Mountant. The 100× oil immersion lens of the Nikon A1R confocal microscope (Nikon, Tokyo, Japan) was used to image samples (excitation at 488 nm from an argon laser, emission between 500 and 520 nm). Images were taken in a single focal plane. In order to determine platelet adhesion, the numbers of platelets in five random images of each coverslip were counted. Platelets were categorized as spread fully (lamellipodia formed), partially spread (defined as filopodia) or adhered (not spreading). Finally, the relative frequencies of these groups were computed.

Clot retraction

Human PRP was prepared and rested at 30°C for 30 minutes. Red blood cells and ^{62}Gap27 or scrambled peptide were mixed with the PRP. The mixture was adjusted to a final volume of 1 mL with modified Tyrode's-HEPES buffer and incubated for 5 minutes at room temperature. Thrombin (final concentration, 1 U/mL) was added to initiate clot generation. A glass pipette was added to the center of each test tube, around which the clot would form, and samples were placed in an incubator chamber at 37^{o}C. Photographs were taken every 10 minutes and the assay was terminated after 60 minutes at which time the clot in the scrambled peptide-treated samples was seen to have retracted completely. Clot weight was measured as a marker for clot retraction. Clots were removed from the glass pipettes and transferred into the pre-weighed microfuge tubes. Clot mass was determined by subtracting the weight of pre-weighed microfuge tubes from the weight of microfuge tubes containing clot.

***In vitro* thrombus formation under flow**

Whole human blood was incubated with the lipophilic dye DiOC6 (5 µM) at 30 °C for 1 hour. Vena8 BioChip microfluidic channels were coated with type I collagen (100 µg/mL) for 1 hour. Channels were washed with modified Tyrode's-HEPES buffer to remove excess collagen. Whole blood was incubated with ^{62}Gap27 or scrambled peptide for 5 minutes. Then, the blood samples were perfused through the collagen-coated channels at an arteriolar shear rate of 20 dyne/cm^2. An argon laser was used to excite fluorescence (488 nm) and emission was recorded at 500–520 nm. Thrombus formation on the microfluidic chip was observed through the 20x objective of the Nikon A1R confocal microscope. Images of single sections were obtained every second for 600 seconds. Finally, NIS-Elements software (Nikon, Tokyo, Japan) was used to compute the mean thrombus fluorescence intensity.

In vivo thrombus formation

C57BL/6 mice were anaesthetised with intraperitoneally administered atropine (0.25 mg/kg), xylazine (12.5 mg/kg) and ketamine (125 mg/kg). When needed, pentobarbital (5 mg/kg) was used to sustain anesthesia. After the exteriorization of the cremaster muscle and removal of the connective tissue, an incision was made in the muscle, resulting in its adherence as a single layer to the glass slide. A buffer (135 mM NaCl, 4.7 mM KCl, 2.7 mM CaCl2 and 18 mM NaHCO3; pH 7.4) was used to hydrate the muscle.

Before the injury (made with a MicroPoint Ablation Laser Unit; Andor Technology, Belfast, UK), ^{62}Gap27 or scrambled peptide and DyLight® 649-conjugated anti-GPIbα antibody (to label platelets; 0.2 µg/g mouse weight), were introduced into the circulation through a cannula in the carotid artery. After 5 minutes of administration of ^{62}Gap27 or scrambled peptide, the formation of thrombi was observed with an Olympus BX61W1 microscope (Olympus, Tokyo, Japan). A Hamamatsu digital camera (C9300; Hamamatsu Photonics, Welwyn Garden City, UK) with charge-coupled device camera in 640×480 format was used to obtain images before and after injury. The images were analyzed with SlideBook 6 software (Intelligent Imaging Innovations, Denver, CO, USA). The protocol from the Home Office license was followed for the sacrifice of the mice. The protocol was also approved by the Animal Welfare and Ethics Research Board and the University of Reading local ethics review panel.

Tail Bleeding Assay

C57BL/6 mice were anesthetized by intraperitoneal administration of xylazine (12.5 mg/kg) and ketamine (125 mg/kg). ^{62}Gap27 or scrambled peptide was administered through injection via the femoral vein. After 5 minutes of infusion, the tips of the tails (0.3 cm) were cut with a scalpel and immediately placed in tubes with saline in a manner that prevented the cut ends of the tails from touching the walls of the tubes. The bleeding time was recorded until blood flow stopped or for up to 20 minutes. The mice were sacrificed according to the protocol that was approved by the University of Reading local ethics review panel, the Animal Welfare and Ethics Research Board and the Home Office.

cAMP ELISA

A cAMP immunoassay kit based on a competitive ELISA (Cell Signaling Technology, Hitchin, UK) was used to assess cAMP levels, according to the protocol provided by the manufacturer. Washed platelets (4×10^8 cell/mL) were added to a glass cuvette and treated with ^{62}Gap27 or scrambled peptide for 5 minutes. After 5 minutes of stimulation with CRP-XL or thrombin, lysis buffer (Triton™ X-100: 1% polyethylene glycol octylphenol ether) was added to the samples. The samples were immediately frozen at −20°C. The samples were later thawed and added to microwells coated with cAMP XP® rabbit monoclonal antibody. The association between cAMP concentration and absorbance was determined using cAMP standards. The assay plate was covered and incubated on a horizontal orbital plate shaker for 3 hours at room temperature. After incubation, the contents of the wells were removed and the wells were washed with 1x washing buffer three times. Then, 3,3',5,5'-tetramethylbenzidine substrate was added to the wells and the plate was incubated for 30 minutes. Stop solution was added to terminate the reaction. The absorbance at 450 nm was periodically determined with a NOVOstar plate reader (BMG Labtech, Aylesbury, UK). A standard curve was plotted from the absorbance readings of the cAMP standards. cAMP concentrations were computed for the test sample readings via the inverse function.

Western blotting

To study cell signaling, human or mouse washed platelets were prepared at a density of $4x10^8$ cells/ml under non-aggregation conditions [indomethacin (20 µM), cangrelor (1 µM), MRS2179 (100 µM) and EGTA (1 mM). These platelets were treated with an inhibitor of Cx function or scrambled peptide control for 5 minutes and then stimulated with platelet agonists in the aggregometer. Unstimulated or stimulated samples were lysed with 6X Laemmli sample reducing buffer and heated to 95^{o}C for 5 minutes before storing at -20^{o}C until use.

The proteins in the extracts of the platelet lysates were separated by SDS-polyacrylamide gel electrophoresis (PAGE) after heating to 95°C for 10 minutes in 6x Laemmli reducing buffer. The samples and molecular weight standards were loaded onto 4%–20% acrylamide gradient gels (Bio-Rad precast gels; Bio-Rad, Watford, UK). The gels were run at a constant voltage (100 V) for 90 minutes in a Mini-PROTEAN® II apparatus (Bio-Rad, Watford, UK) with Tris-glycine buffer in the

running reservoir. The separated proteins were transferred to PVDF membranes (Bio-Rad, Watford, UK) by semi-dry transfer. PVDF membranes, soaked in methanol, were placed under the resolving gels. Four sheets of 3-mm filter paper soaked in anode buffer (300 mM Tris base and 20% [v/v] methanol; pH 10.4) were placed below the membranes and 4 sheets of 3-mm filter paper soaked in cathode buffer (25 mM Tris base and 40 mM 6-amino-n-hexanoic acid; pH 9.4) were placed above the resolving gels. The proteins were transferred from the gels to the membranes by applying a constant voltage (15V) for 2 hours.

The PVDF membranes were blocked with 5% (w/v) BSA dissolved in 1% (v/v) Tris-buffered saline–TWEEN® 20 for 1 hour at room temperature. The membranes were incubated with the primary antibodies, which were diluted in 1% (v/v) TBST with 2% (w/v) BSA, overnight at 4°C. After overnight incubation, the membranes were washed with TBST (3 × 5 minutes) to remove unbound antibodies. Fluorescently labeled secondary antibodies diluted in 1% (v/v) TBST containing 2% (w/v) BSA were then applied to the membranes, which were incubated for 1 hour at room temperature in the dark. The membranes were then washed with TBST (3 × 5 minutes) and their fluorescence visualized using a Typhoon FLA 9500 fluroimager (Amersham Biosciences, Buckinghamshire, UK). Image Quant software version 8.1 (GE Healthcare) was used to quantify the fluorescence intensities of the individual bands.

Supplemental Figure 1

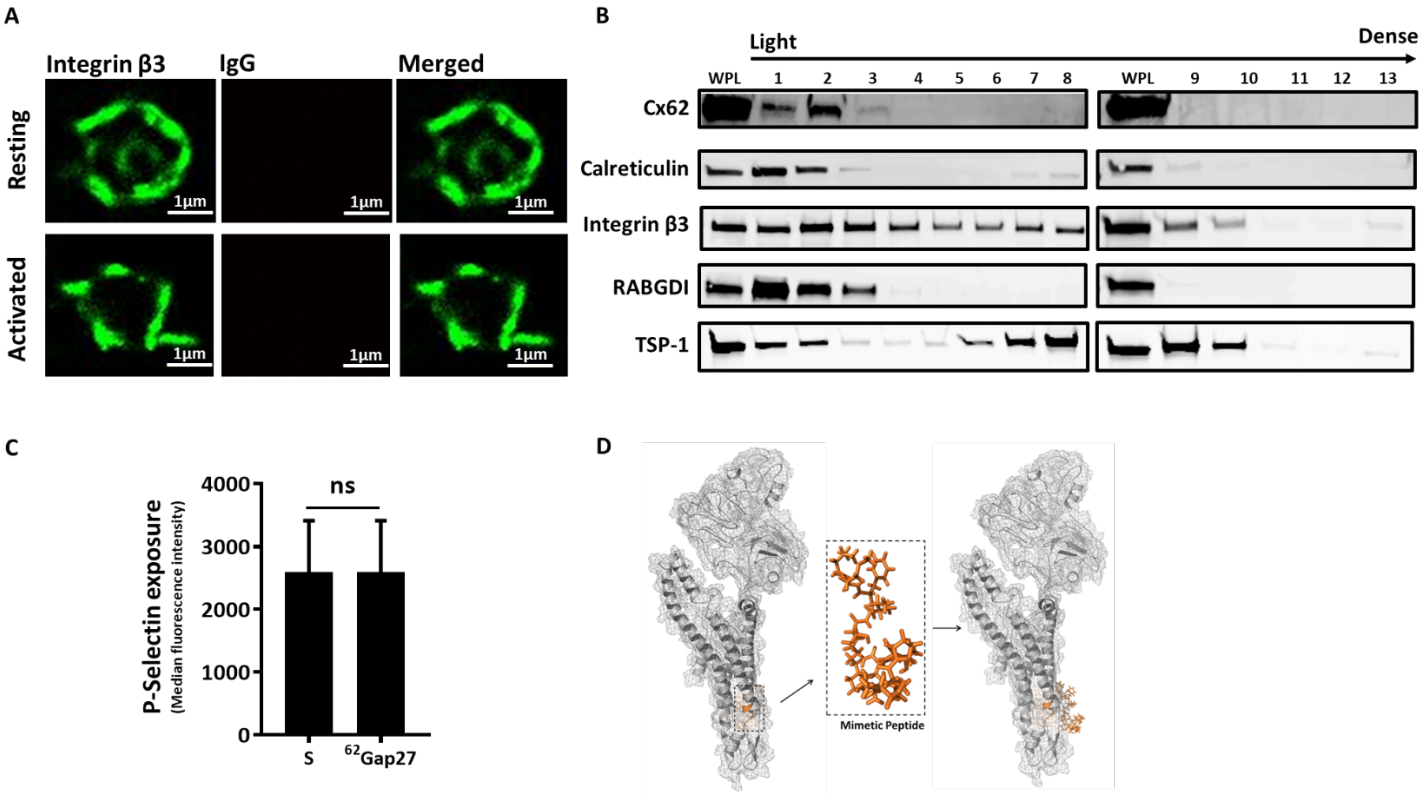

Supplemental Figure 1. Localization of Cx62 in platelets. (A) Treatment of platelets with secondary antibody alone (in the absence of anti-GJA10 primary antibody) was performed during STORM microscopy to exclude the possibility of non-specific staining **(B)** Cx62 is distributed in low-density subcellular platelet fractions. Ultracentrifugation was utilized to separate platelet homogenates on a sucrose density gradient. The fractions were separated by SDS-PAGE and immunoblotted for Cx62, β3 integrin, calreticulin, RabGDIb and TSP-1. The lower-density platelet fractions (lanes 1–6) are identified by the DTS protein calreticulin, surface marker integrin β3, and the cytosolic marker RabGDIb. The α-granule protein TSP-1 was used to identify the heavier fractions. A Typhoon™ FLA 9500 fluorimager was utilized to examine the immunoblots (GE Healthcare, UK). The results are representative of 3 individual experiments. WPL: whole platelet lysate. **(C)** Effects of ^{62}Gap27 (100 μg/ml) on thrombin (0.1 U/ml) mediated P-selectin exposure, in comparison to the scrambled peptide (S; 100 μg/ml) was evaluated using flow cytometry. **(D)** Structural representation of the target region to which the ^{62}Gap27 mimetic peptide was designed, and the putative binding site of the inhibitor on Cx62.Statistical analysis was performed using the student t-test.

Supplemental Figure 2

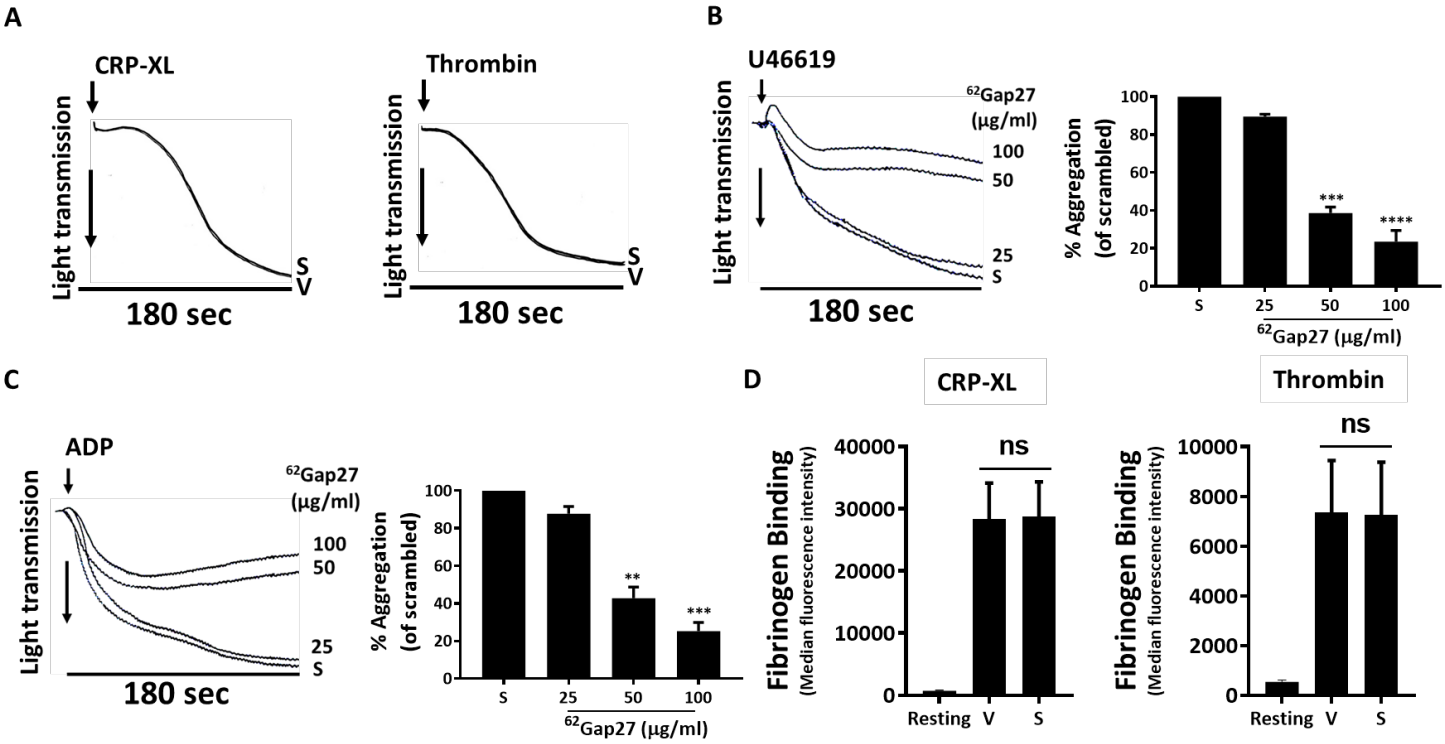

Supplemental Figure 2. ^{62}Gap27 inhibits platelet aggregation and fibrinogen binding to integrin αIIbβ3. **(A)** Washed human platelets (4×10^8 cells/mL) were treated with vehicle (V; ddH_2O) or scrambled peptide (S; 100 µg/ml) and stimulated with CRP-XL or thrombin. Aggregation was measured using optical light transmission aggregometry for 180 seconds. Representative aggregation traces are shown **(B, C)** Washed human platelets (4×10^8 cells/mL) were treated with ^{62}Gap27 or scrambled peptide (100 µg/ml) for 5 minutes prior to their stimulation with **(B)** U46619 (EC_{50}: 0.25–0.4 µM) or **(C)** ADP (EC_{50}: 5–10 µM). Aggregation was measured optical light transmission aggregometry for 180 seconds. Representative aggregation traces and quantified data shown (Scrambled-treated samples represent 100% aggregation) **(D)** Effects of the vehicle (V; ddH_2O) and scrambled peptide (S; 100 µg/ml) on CRP-XL (0.25 µg/ml) and thrombin (0.05 U/ml) mediated fibrinogen binding was evaluated in platelets (in PRP) using flow cytometry. Data represent mean ± SEM (n≥3), **P<0.01, ***P<0.001 and ****P<0.0001 was calculated by one-way ANOVA.

Supplemental Figure 3

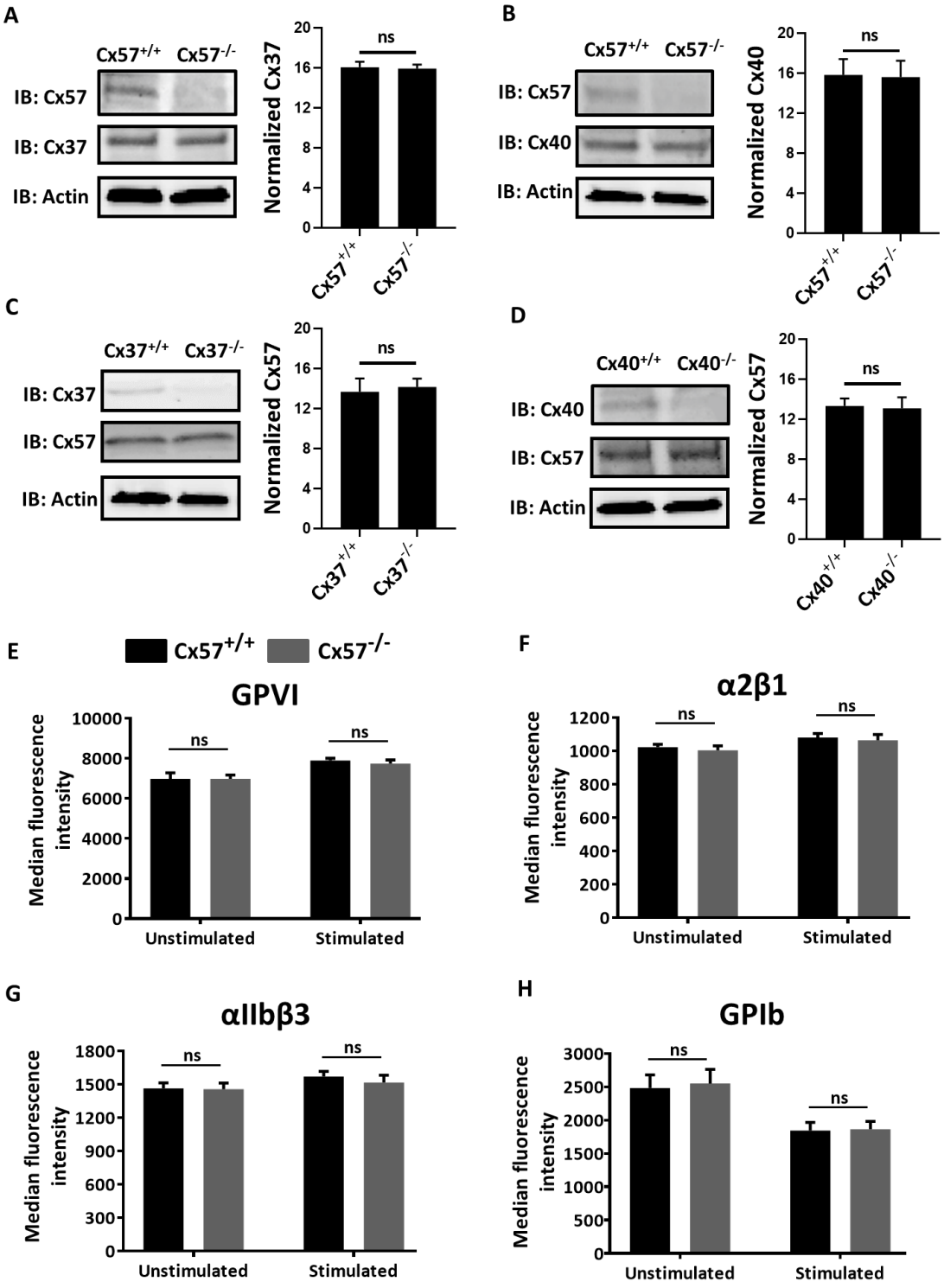

Supplemental Figure 3. Characterization of Cx57$^{-/-}$ platelets. Cx57$^{+/+}$ and Cx57$^{-/-}$ platelets were used to evaluate the expression of **(A)** Cx37 and **(B)** Cx40 by immunoblotting. **(C)** Cx37$^{+/+}$, Cx37$^{-/-}$ and **(D)** Cx40$^{+/+}$,

$Cx40^{-/-}$ platelets were used to analyze the expression of Cx57 by immunoblotting. Actin was used as a loading control. Quantified data shown. The expression levels of **(E)** GPVI **(F)** α2β1, **(G)** αIIbβ3 and **(H)** GPIb were analyzed in resting and CRP-XL-activated (1 µg/ml) platelets from $Cx57^{+/+}$ and $Cx57^{-/-}$ mice by flow cytometry. The student t-test was used for statistical analysis.

Supplemental Figure 4

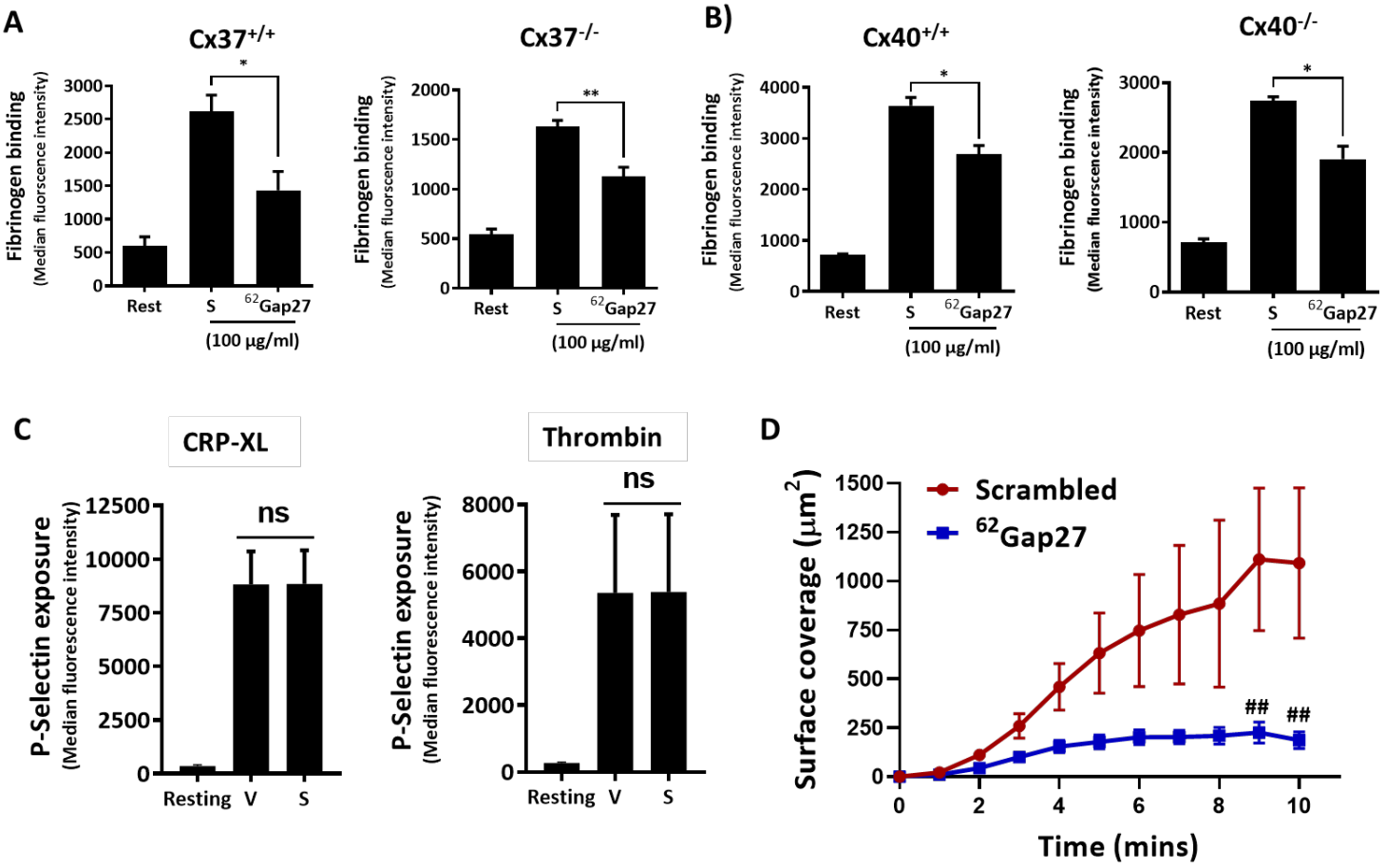

Supplemental Figure 4. Cx57 functions independently of Cx37 and Cx40 in platelets. PRP from **(A)** $Cx37^{+/+}$ and $Cx37^{-/-}$ and **(B)** $Cx40^{+/+}$ and $Cx40^{-/-}$ mice was treated with ^{62}Gap27 (100 µg/ml) or scrambled peptide (S; 100 µg/ml) for 5 minutes. Fibrinogen binding levels were evaluated after stimulation with CRP-XL (1 µg/ml). **(C)** Effects of scrambled peptide (S; 100 µg/ml) and vehicle (V: ddH_20) on CRP-XL (0.25 µg/ml) and thrombin (0.05 U/ml) mediated P-selectin exposure was evaluated in platelets (in PRP) using flow cytometry. **(D)** DiOC6-loaded human whole blood was treated with scrambled peptide or ^{62}Gap27 (100 µg/ml) for 5 min before perfusion through collagen-coated (100 µg/mL) Vena8Biochips at a shear rate of 500 s^{-1} (20 dyne/cm^2). Quantified data display surface coverage of thrombus over a period of 10 minutes. Data represent mean ± SEM (n≥3). *P<0.05 and **P<0.01 was calculated by the Student t-test. ##P<0.01 was calculated by two-way ANOVA.

Supplemental Figure 5

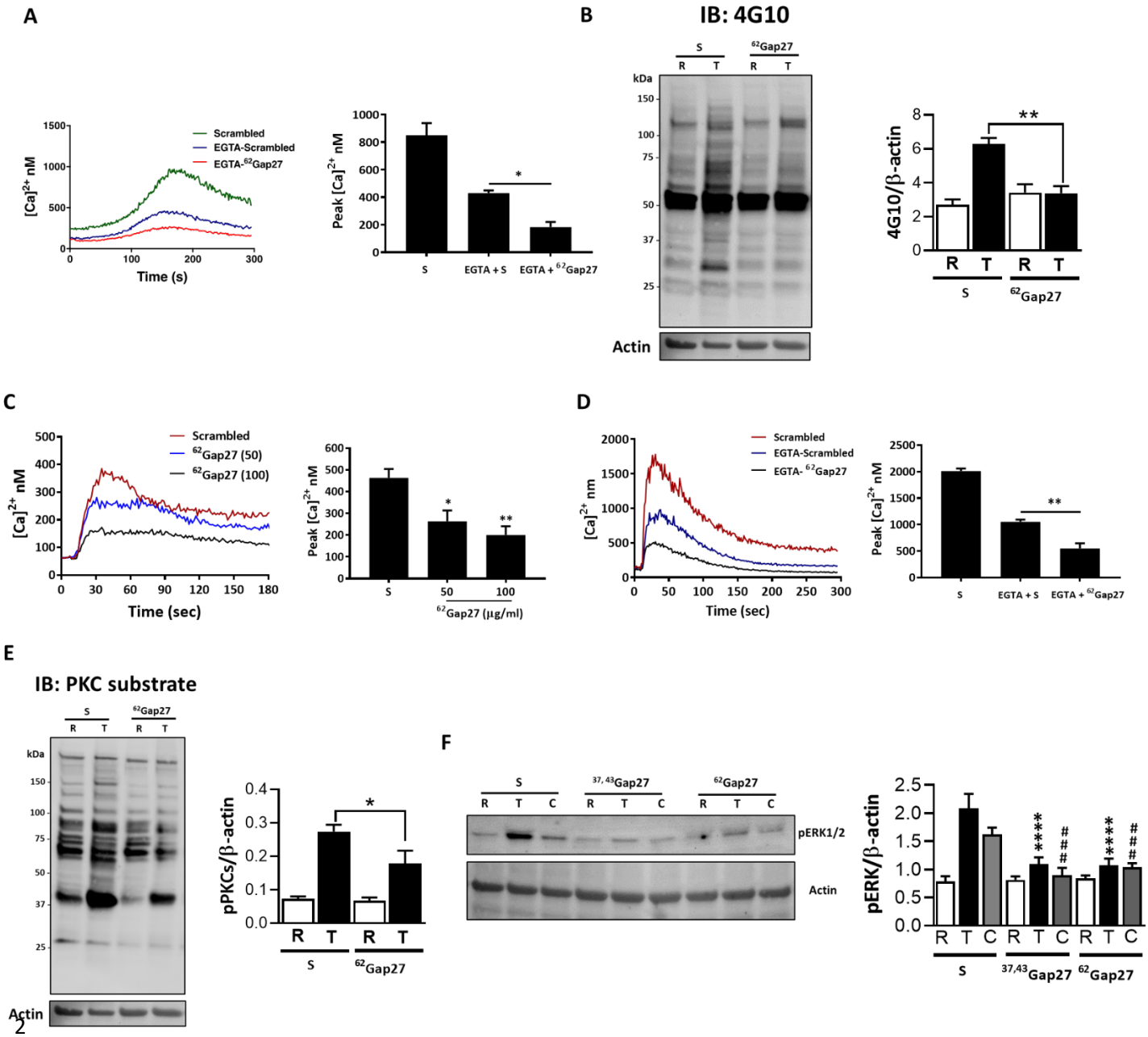

Supplemental Figure 5. ^{62}Gap27 inhibits thrombin-mediated signaling in human platelets. (A) Fura-2AM-loaded washed platelets (4×10^8 cells/mL) were incubated with ^{62}Gap27 (50 or 100 µg/mL) or scrambled peptide (S, 100 µg/mL) for 5 minutes in the presence of EGTA and stimulated with CRP-XL (0.5 µg/mL) for 5 minutes. Spectrofluorimetry was used to measure the release of calcium from intracellular stores. Representative traces of calcium mobilization over a period of 5 minutes and quantified data (peak calcium levels) are shown. **(B)** Representative blot and quantified data indicate the levels of phosphorylated total tyrosine in washed human platelets (4×10^8 cells/mL). Resting human platelets (R) were pre-incubated with scrambled peptide (S) or ^{62}Gap27 (100 µg/mL) for 5 min then were stimulated with thrombin (T; 0.05 U/ml). **(C)** Calcium mobilization and **(D)** release of calcium from intracellular stores was measured in Fura-2AM-loaded washed platelets (4×10^8 cells/mL) treated with scrambled peptide (S; 100 µg/mL) or ^{62}Gap27 and stimulated with thrombin (0.05 U/ml). Representative traces of calcium mobilization over a period of 5 minutes and quantified data (peak calcium levels) are shown. **(E)** Representative blot and quantified data indicate the levels of phosphorylated PKC substrate in washed human platelets (4×10^8 cells/mL). Resting human platelets (R) were pre-incubated with scrambled peptide (S) or ^{62}Gap27 (100 µg/mL) for 5 min then were stimulated with thrombin (T; 0.05 U/ml). **(F)** Representative blot and quantified data indicate the levels of pERK1/2 in washed human platelets (4×10^8 cells/mL). Resting human platelets (R) were pre-incubated for 5 minutes with Scrambled peptide (S) or ^{37,43}Gap27 or ^{62}Gap27 (100 µg/mL) and stimulated with thrombin (T; 0.05 U/ml) or CRP-XL (C; 1 µg/ml). Actin was used as a loading control. Data represent the mean ± SEM (n≥3). *P<0.05, **P<0.01, ****P<0.0001 and ####P<0.0001 was calculated by one-way ANOVA.

Supplemental Figure 6

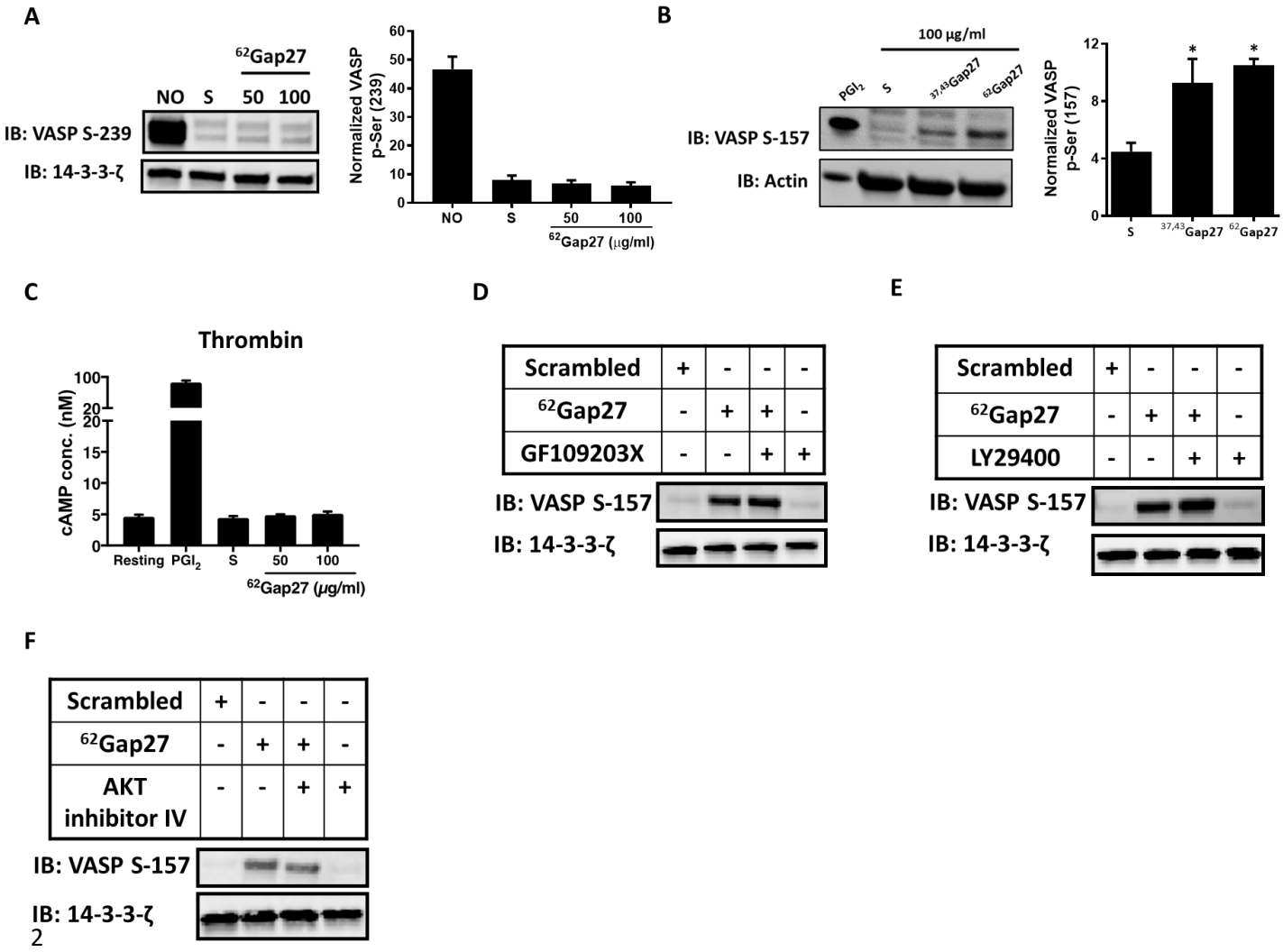

Supplemental Figure 6. ^{62}Gap27 modulates PKA activity. (A) Resting washed human platelets (4×10^8 cells/mL) treated with scrambled peptide (S; 100 μg/mL) or ^{62}Gap27 (50 and 100 μg/mL) for 5 minutes were tested for VASP S239 phosphorylation (a marker of PKG activity). Platelets treated with PAPA-Noeate (NO; 100 μM) for the stimulation of PKG-mediated phosphorylation were used as positive controls. **(C)** Resting washed human platelets (4×10^8 cells/mL) treated with scrambled peptide (S) or ^{37,43}Gap27 or ^{62}Gap27 (100 μg/mL) for 5 minutes were tested for VASP S157 phosphorylation. Platelets treated with PGI_2 (1 μg/mL) were used as a positive control. **(D)** Resting washed human platelets (4×10^8 cells/mL) were treated with GF109203X (10 μM), **(E)** LY29400 (100 μM) or **(F)** AKT inhibitor IV (5 μM) for 15 minutes before incubation with the scrambled peptide or ^{62}Gap27 (100 μg/mL) for 5 minutes. Samples were assayed for VASP-S157 phosphorylation. 14-3-3-ζ was detected by immunoblotting as a loading control. Representative blots are shown. Data represent the mean ± SEM (n≥3). *P<0.05 was calculated by one-way.

References

1. Spyridon M, Moraes LA, Jones CI, et al. LXR as a novel antithrombotic target. *Blood*. 2011;117(21):5751-5761.

2. Unsworth AJ, Flora GD, Sasikumar P, et al. RXR Ligands Negatively Regulate Thrombosis and Hemostasis. *Arterioscler Thromb Vasc Biol*. 2017;37(5):812-822.

3. Flora GD, Sahli KA, Sasikumar P, et al. Non-genomic effects of the Pregnane X Receptor negatively regulate platelet functions, thrombosis and haemostasis. *Sci Rep*. 2019;9(1):17210.

4. Jonnalagadda D, Sunkara M, Morris AJ, Whiteheart SW. Granule-mediated release of sphingosine-1-phosphate by activated platelets. *Biochim Biophys Acta*. 2014;1841(11):1581-1589.

5. Malkusch S, Endesfelder U, Mondry J, Gelleri M, Verveer PJ, Heilemann M. Coordinate-based colocalization analysis of single-molecule localization microscopy data. *Histochem Cell Biol*. 2012;137(1):1-10.

6. Ovesný M, Křížek P, Borkovec J, Svindrych Z, Hagen GM. ThunderSTORM: a comprehensive ImageJ plug-in for PALM and STORM data analysis and super-resolution imaging. *Bioinformatics*. 2014;30(16):2389-2390.

7. Taylor KA, Wright JR, Vial C, Evans RJ, Mahaut-Smith MP. Amplification of human platelet activation by surface pannexin-1 channels. *J Thromb Haemost*. 2014;12(6):987-998.

8. Vaiyapuri S, Jones CI, Sasikumar P, et al. Gap junctions and connexin hemichannels underpin hemostasis and thrombosis. *Circulation*. 2012;125(20):2479-2491.

9. Lalo U, Allsopp RC, Mahaut-Smith MP, Evans RJ. P2X1 receptor mobility and trafficking; regulation by receptor insertion and activation. *J Neurochem*. 2010;113(5):1177-1187.

10. Sayers EW, Cavanaugh M, Clark K, Ostell J, Pruitt KD, Karsch-Mizrachi I. GenBank. *Nucleic Acids Res*. 2019;47(D1):D94-D99.

11. Wilkins MR, Gasteiger E, Bairoch A, et al. Protein identification and analysis tools in the ExPASy server. *Methods Mol Biol*. 1999;112:531-552.

12. McGuffin LJ, Shuid AN, Kempster R, et al. Accurate template-based modeling in CASP12 using the IntFOLD4-TS, ModFOLD6, and ReFOLD methods. *Proteins*. 2018;86 Suppl 1:335-344.

13. McGuffin LJ, Atkins JD, Salehe BR, Shuid AN, Roche DB. IntFOLD: an integrated server for modelling protein structures and functions from amino acid sequences. *Nucleic Acids Res*. 2015;43(W1):W169-173.

14. Maghrabi AHA, McGuffin LJ. ModFOLD6: an accurate web server for the global and local quality estimation of 3D protein models. *Nucleic Acids Res*. 2017;45(W1):W416-w421.

15. Grosdidier A, Zoete V, Michielin O. SwissDock, a protein-small molecule docking web service based on EADock DSS. *Nucleic Acids Res*. 2011;39(Web Server issue):W270-277.

16. Krissinel E, Henrick K. Inference of macromolecular assemblies from crystalline state. *J Mol Biol*. 2007;372(3):774-797.